AALBORG UNIVERSITY
STUDENT REPORT

P10, Fall 2016 – Spring 2017

ToA Path Estimation for Indoor Positioning

Using MUSIC algorithm for Time Resolution Enhancement

WCS10 - Group 1051

8th June 2017

Antennas, Propagation and Radio Networking (APNet) Department of Electronic Systems
Fredrik Bajers Vej 7
DK-9220 Aalborg Ø
http://es.aau.dk

AALBORG UNIVERSITY
STUDENT REPORT

Title:
ToA Path Estimation for Indoor Positioning
Using MUSIC algorithm for Time Resolution Enhancment

Theme:
Wireless Communication Systems

Project Period:
P10, Fall 2016 - spring 2017

Project Group:
1051

Author:
Mathias Hjorth Laursen

Supervisor:
Troels Bundgaard Sørensen

Pages: 71

Date of Completion:
8th June 2017

Abstract:

Due to the increasing demand for indoor positioning or navigation systems this thesis investigates the possibilities of creating an indoor positioning system using a combination of ToA and the MUSIC algorithm for increased time resolution. The characteristics of the wireless transmission channel are investigated as these can be used for creating end evaluating an indoor positioning system.
A model describing a ToA system is developed. Simulations of this model was made in order to evaluate the impact of different wireless characteristics, especially the ToA between different reflected signal paths and the improvements made by the MUSIC algorithm. Measurements were made to evaluate the performance of the MUSIC algorithm on a wireless channel in LOS and NLOS scenarios. Test results shows a significant improvement by using a combination of ToA and the MUSIC algorithm compared with a traditional ToA positioning system.

Preface

The following master thesis covers the project made by Mathias Laursen to complete his Wireless Communication Systems Master's program at Aalborg university. The topic of the thesis is indoor localisation based on wireless channel characteristics and complex computation algorithm to enhance accuracy.

The author would like to thank Thomas Lundgaard Hansen for his help within the field of signal processing.

The report is divided into 2 overall parts, first chapter 1-3 introduces the concept of indoor localisation together with a basic evaluation of different wireless channel characteristics to use for position estimation. Following chapter 4-5 describes a system model for simulating Time of Arrival as a wireless channel characteristic to improve the accuracy of indoor location system by using the MUSIC algorithm to enhance the time resolution of a measured wireless channel. Part to results in an evaluation of empirical and simulated wireless channels and the ability to make precise positioning using time of arrival.

Citations are made by the use of American Institute of Physics (AIP) style. This style represents a citation by the use of only a number e.g. [13] which refers to the 13.th entry in the bibliography found in the end of the thesis. Adding the number before a full stop e.g. a dot as "[ ]." the citation refers only to that sentence and adding it after full stop the citation is referring for the full paragraph.

For table, figure and equation references the following approach is used e.g. figure x,y refers to the y'th figure in chapter x. Similar for the table and equations.

Aalborg University, Denmark, June 8th 2017.

Contents

Abbreviations

AoA angle of arrival
AWGN additive white gaussion noise
CDF cumulative distribution function
DDE distance determination error
DDP dominant direct path
EVD eigenvalue decomposition
FCF frequency correlation function
GPS global positioning system
IPS indoor positioning system
kNN k-Nearest Neighbour
LOS line of sight
MT mobile terminal
MUSIC MUltiple SIgnal Classification
NDDP non dominant direct path
NLOS no line of sight
PDE Position determination error
PRN pseudo random noise
RSSI received signal strength indicator
RTT round trip time
TDoA time difference of arrival
ToA time of arrival
ToF time of flight
UDP undetected direct path
UWB Ultra Wideband
WSSUS wide sense stationary uncorrelated scattering

List of Symbols

A amplitude

α attenuation

B bandwidth

c speed of light

h channel impulse response

d true distance

Δt time difference

d_{err} synchronization error

$\hat{d}$ distance estimate

δ dirac pulse

μ_θ mean angular distribution

$\hat{p}$ position estimate

p true position

σ_θ angular standard deviation

τ propagation delay

θ angle

t_{travel} time traveled

Chapter 1

Introduction

1.1 Background

In recent years the usage of positioning data has increased in a variety of applications. Often outdoor applications perform well by utilising global positioning system (GPS) or similar outdoor positioning systems. However for the application of indoor localisation or navigation the GPS system does not provide satisfying accuracy. To achieve high accuracy in an indoor environment a dedicated system has to be created which takes into account the complexity of an indoor environment.

The need for indoor positioning systems is a increasingly growing market [1].

Indoor positioning system (IPS) has a wide range of applications and application areas. Below are listed some different scenarios where localisation could provide increased customer experience, ease of work, or new application could be designed based on position knowledge. Such systems could be tracking positions or navigation:

- In the healthcare industry an accurate localisation system could provide easier patients tracking for hospitals, or for tracking demented people. Similar the system could be used for localising staff or equipment, or help patients and relatives navigate the area.
- For places like airports, museums or subways a localisation system can also help provide guidance. This could be for guiding people to their gates in the airports, the correct train in the subway or grant a guided tour through museums and similar.
- In warehouses the system could be used for tracking incoming and outgoing packets/orders/etc. And to keep the location of different wares known, so that packing of orders eases. In larger warehouses or factories, localisations of tools or different machines would also possible.
- At shopping malls or grocery stores a tracking system could also help people find the different wares they are searching, or the system could in cooperation with a shopping list, create the fastest way through the stores to get all wares listed.
- Lastly an IPS can be used for gathering positioning data for all kind of different

locations. This could help provide a lot of statistical usage and applications. e.g. knowing the positions of customers in a shopping mall, grants the possibility for placing different wares strategically to sell more.

The need for more advanced and accurate positioning systems than those already designed is needed. The systems already designed are based on a set of different technologies that can be used to create an IPS. A list of technologies is found below [2].

- Satellite based navigation
- Inertial navigation system
- Sound based navigation
- Optical based navigation
- Electromagnetic wave based navigation
- Magnetic based navigation
- Infrastructure system based navigation

From surveys of IPS [2,3], it is seen that technologies for indoor positioning is mostly based on acoustics or radio frequency methods. For the rest of the project, the main focus will be on RF technology for indoor localisation. The graph found on fig. 1.1 from [3] provides an outline of the accuracies and areas of usage for different wireless based localisation systems.

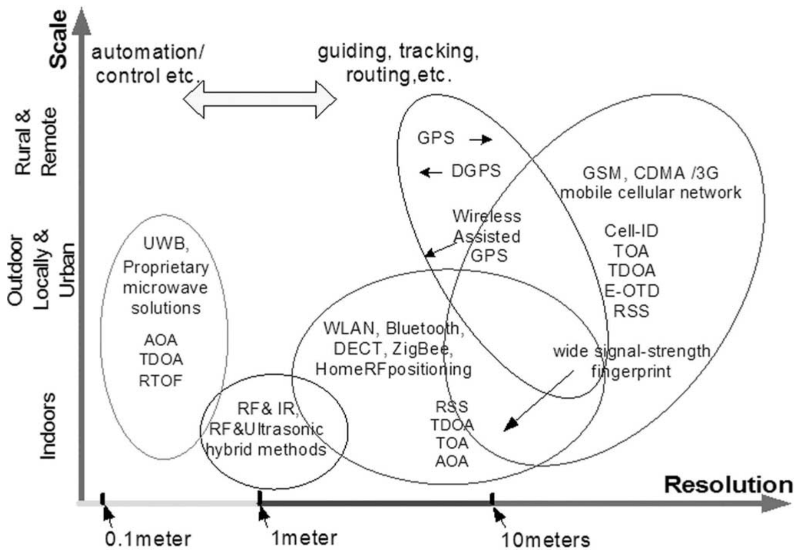

Figure 1.1: *Outline of current wireless localisation systems. Figure from [3].*

Similar [3] have also evaluated a set of different IPS. Figure 1.2 shows the results and listing among others, the accuracy, precision and wireless technology used.

System/ Solution	Wireless technologies	Positioning algorithm	Accuracy	Precision	Complexity	Scalability/ Space dimension	Robust-ness	Cost
Microsoft RADAR [35, 36]	WLAN, Received Signal Strength (RSS)	*K* NN, Viterbi-like algorithm	3~5m	50%within around 2.5 m and 90% within around 5.9 m	Moderate	Good /2D,3D	Good	Low
Horus [37,38]	WLAN RSS	Probabilistic method	2m	90% within 2.1m	Moderate	Good/2D	Good	Low
DIT [41, 19]	WLAN RSS	MLP, SVM, etc.	3m	90% within 5.12m for SVM; 90% within 5.40m for MLP	Moderate	Good/2D,3D	Good	Low
Ekahau[11]	WALN RSSI	Probabilistic method (Tracking-assistant)	1m	50% within 2m	Moderate	Good/2D	Good	Low
SnapTrack[1]	Assisted GPS, TDOA		5m-50m	50% within 25m	High	Good/2D,3D	Poor	Medium
WhereNet[14]	UHF TDOA	Least Square/ RWGH	2-3m	50% within 3m	Moderate	Very good / 2D,3D	Good	Low
Ubisense[8]	unidirectional UWB TDOA+ AOA	Least Square	15cm	99% within 0.3m	Real time response (1Hz – 10 Hz)	2-4 sensors per cell (100-1000m); 1 UbiTag per object /2D,3D	Poor	Medium to High
Sappire Dart[19]	unidirectional UWB TDOA	Least Square	<0.3m	50% within 0.3m	response frequency (0.1Hz – 1Hz)	Good/2D, 3D	Poor	Medium to High
SmartLOCUS [58]	WLAN(RSS) + Ultrasound(RTOF)	N/A	2-15cm	50% within 15cm	Medium	Good/2D	Good	Medium to High
EIRIS[18]	IR + UHF (RSS) + LF	Based on PD	<1m	50% within 1m	Medium to High	Good/2D	Poor	Medium to High
SpotON [28]	Active RFID RSS	Ad-Hoc lateration	Depends on cluster size	N/A	Medium	Cluster at least 2 Tags/2D	Good	Low
LANDMARC [29]	Active RFID RSS	KNN	<2m	50% within 1m	Medium	Nodes placed densely	Poor	Low
TOPAZ [13]	Bluetooth (RSS) + IR	Based on PD	2m	95% within 2m	positioning delay 15-30s	Nodes placed every 2-15 m	Poor	Medium
MPS[15]	QDMA	Ad-Hoc lateration	10m	50% within 10m	1s	Excellent/2D,3D	Good	Medium
GPPS[61]	DECT cellular system	Gaussian process (GP), *k*NN	7.5 m for GP; 7 m for *k*NN	50% within 7.3m	Medium	Good/2D	Good	Medium
Robot-based[44, 46, 49]	WLAN (RSS)	Bayesian approach	1.5 m	Over 50% within 1.5m	Medium	Good/2D	Good	Medium
MultiLoc [74]	WLAN (RSS)	SMP	2.7 m	50% within 2.7m	Low	Good/2D	Good	Medium
TIX [75]	WLAN (RSS)	TIX	5.4 m	50% within 5.4m	Low	Good/2D	Good	Medium
PinPoint 3D-ID [57]	UHF (40MHz) (RTOF)	Bayesian approach	1 m	50% within 1m	5s	Good/2D,3D	Good	Low
GSM fingerprinting[31]	GSM cellular network (RSS)	Weighted *k*NN	5 m	80% within 10m	Medium	Excellent / 2D,3D	Good	Medium

Figure 1.2: *Wireless indoor positioning survey evaluated in [3].*

Looking at fig. 1.2 it is concluded that RSS implementation for IPS is a bad choice for direct implementation, as the accuracy for these systems is within 2-5 m with only two systems obtaining accuracies below this. Time based systems seems like the best choice for an IPS system, as the accuracies for these system is around 1 m when using an Ultra Wideband (UWB) system. Systems based on more than one technology seems to achieve higher accuracies than those based only on a single technology e.g. the SmartLOCUS system which is based on both RF time of arrival (ToA) and Ultrasound ToA achieves an accuracy of <15 cm [4].

1.2 Thesis Contribution

The contribution of the thesis is an evaluation of a method to obtain accurate position estimates by exploiting the signal properties for the ToA of wireless channels. First an evaluation is performed to isolate what initially seems to be the best wireless characteristic for creating an IPS. Afterwards this characteristic is further analysed and the high resolution MUSIC algorithm is used to further improve the position detection ability. Measurement and evaluations of the wireless channel in different LOS and NLOS are evaluated w.r.t. the MUSIC signal processing algorithm. Different input parameters for the complex algorithm are evaluated to measure the performance in the different LOS and NLOS scenarios. Paremeters tested are SNR, samples, bandwidth and specific parameter estimation for the MUSIC algorithm.

1.3 Thesis Overview

The remaining chapters for the thesis will be as follows; Chapter 2 describes the basic terms used in localisation, afterwards is a description of the different localisation methods which can be utilised for calculating a position and the chapter ends with a description of the different wireless channel characteristics that can be utilised to obtain input data for the localisation methods. Chapter 3 evaluates the input data and the errors introduced by these due to changes in the wireless channel. From the conclusion that the ToA system seems to achieve best performance, chapter 4 describes a ToA system model and how to measure this. After the high resolution algorithm is described. Section 5.1 describes the evaluation of the MUSIC algorithm w.r.t. the different parameters that changes the performance of this. Both simulated and empirical data is evaluated. Chapter 6 concludes the project and describes future work which could be made.

Chapter 2

Indoor Localisation

The following chapter is structured as follows. Section 2.1 will provide an overview of the different terms used in the project. Section 2.2 provides an overview of the different positioning methods used e.g. lateration and fingerprinting. Section 2.3 explains the different wireless characteristics which can be used to obtain data for the positioning methods. Section 2.4 describes the performance measure for the different IPS examined.

2.1 Definition Overview

To better understand what an indoor positioning system(IPS) is, it is important to know the most commonly used expressions and definitions.

Tag is used to describe the transmitting/receiving devices mounted on people or equipment to track locations. The tag is both used for description of a dummy-transmitting device and a smart device, which could include both transmitting, receiving and calculating capabilities. It is also known as a mobile terminal (MT) or a transceiver.

Nodes are the devices, which receives the transmitted signal from the tag, or in some situations transmits a signal to the tag. The nodes also in most cases calculates the position of the tag or forwards the data to a server, depending on the system architecture. Nodes are placed in known positions for the system to have reference points when calculating the tag position. In other context the nodes are denoted base stations, reference points or gateways.

IPS can be created in different fashions, most commonly it consists of a set of tags (the devices which location /position are wanted) and a set of nodes which are reference points and the sampling system used to estimate the position of the tags. IPS is used to denote a system which is capable of locating people or objects in an indoor environment mounted with tags. The positioning capability is measured both by accuracy and precision of the system.

Accuracy is the mean distance error between estimated locations and the true locations. Accuracy describes how far off the mean from a set of measurements is from the true location, thereby it can be seen as a offset error in the IPS. The accuracy of a system is closely related to, but it not equal to the precision.

Precision is a consideration of how robust a system is. The precision is often refereed to as the standard deviation of the location estimates or the standard deviation of the accuracy. Compared with accuracy, a system can be very accurate and have very low mean estimation error, however the position estimates used to obtain the mean estimation error, can be both precise and imprecise. If the system is precise the deviation from the estimated position is very low, and for an imprecise system the deviation from estimate is high. Both accuracy and precision can be seen on fig. 2.1.

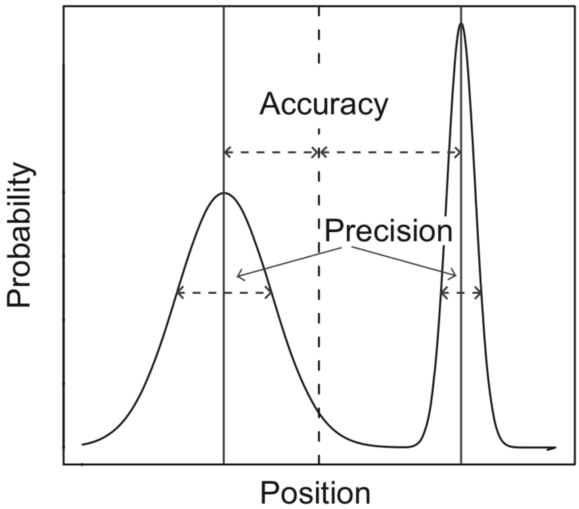

Figure 2.1: *Figure showing difference between accuracy and precision. Figure from [5].*

Complexity as a rule of thumb increases the accuracy, range and precision of a system. However this will decrease other competitive parameters of a system such as the update rate, energy efficiency, setup cost, computations, etc.

Update rate defines the rate at which the IPS updates the position of a tag. The update rate depends on the complexity of the system, the algorithms used for calculating positions, the CPU speed and amount of data to handle.

Line of sight (LOS) is an environmental description stating information of the travel path for a signal. For LOS the direct path between a tag and a node is unobstructed.

No line of sight (NLOS) similar to LOS states information about the environment, however for NLOS the direct path between tag and node is either partially or fully blocked, This condition happens when the direct path from a tag to a node is blocked by an object, this could be a wall, window, furnitures, doors, etc, each assumed to attenuate or block the signal.

LOS and NLOS is further described in appendix B.

2.2 Description of Localisation Methods

The following section will describe the algorithms used for estimating the position of a tag.

Generally in an IPS, the position of a device is calculated in nodes or in a central server, this is to minimize power consumption of the tag. The reason to use a centralised server is often a result of dummy-tags and dummy-nodes which are only used for transmitting and receiving signals, while further handing the received signal to a stronger computational backbone for position calculations.

To calculate the a position estimate, different algorithms can be used. Even though there are a lot of different positioning techniques and systems, they are generally based on the same limited number of algorithms or variations of these [5].

Tree structure of methods for locating a transmitter is presented in fig. 2.2. Overall location detection can be performed by a scene analysis, which includes e.g. fingerprinting. Second is lateration, utilising either angles or distances or a combination of those. Lastly is the proximity detection which utilises nodes with low range, thereby enabling a system which reports the position of a node as the tag position depending on proximity. Following will be a short description of the different methods.

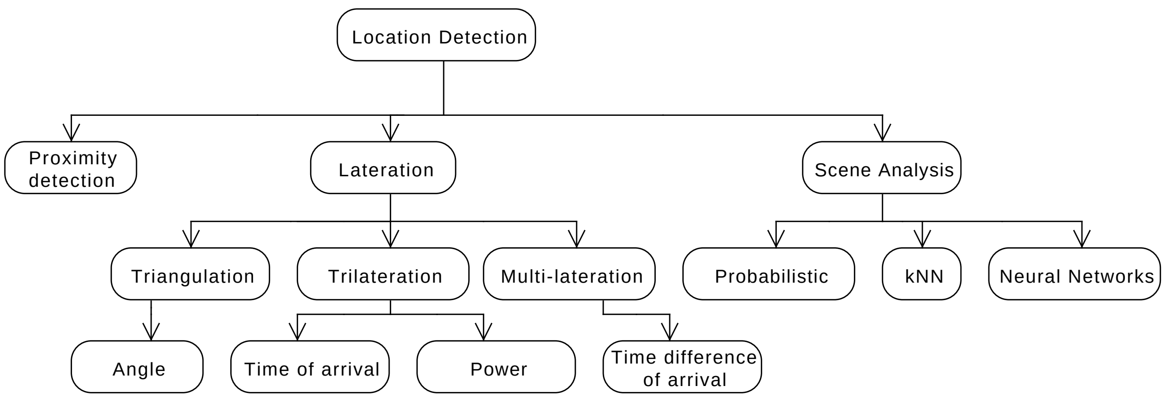

Figure 2.2: *The different classifications for the location detection methods. Scene analysis is also known as fingerprinting. Original figure from [2].*

2.2.1 Proximity Detection

The proximity detection method is also known as connectivity based method. The method of proximity relies on reporting the position of the node, as the estimated position of the tag if the tag is connected with the node. The node which reports tag position, if several nodes has connectivity, is the one with the strongest signal receiption, another measure could also be the one with first detected ToA. Therefore to obtain a high accuracy in a proximity detection system a dense deployed node setup is required with each node having low connection range to avoid ambiguities. An example is given on fig. 2.3, the reported position would be that of "Node1" even though it is clearly seen that the tag is positioned in between "Node1" and "Node2", however as node 1 has strongest connection the position of that node is reported.

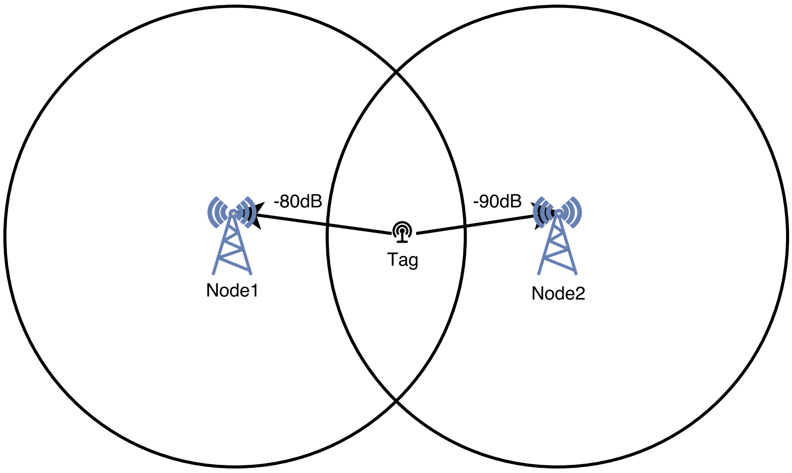

Figure 2.3: *Example of proximity detection. In this case the position is based on the node with strongest receiption.*

2.2.2 Lateration

The method of lateration is to use the geometrics of a triangle to determine the position of a tag from known reference points(nodes). The use of lateration has three variants; triangulation, trilateration and multi-lateration.

Triangulation is the method used for estimating the location of a tag based on angles angle (θ) from reference points. The position of a tag can be estimated using only 2 nodes by knowing the distance d between those and measuring the angle of arrival θ from the transmitting tag, see fig. 2.4.

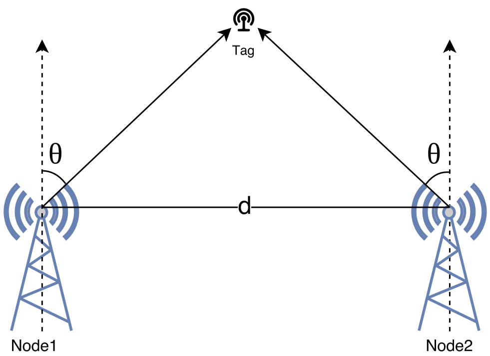

Figure 2.4: *Principle of triangulation*

Trilateration much like triangulation, is an estimation method based on reference points and the geometry of a triangle. Different from triangulation is the usage of distances instead of angles. The distances can be acquired using either ToA methods utilising the signal travel time and the speed at which they travel or by using signal strength reception(power) as a measure of distance. The principle of using trilateration is found on fig. 2.5.

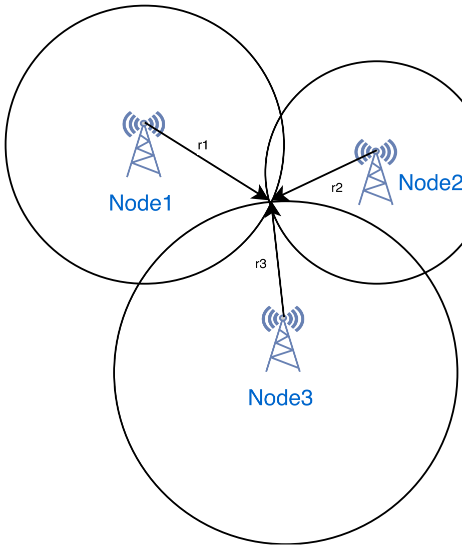

Figure 2.5: *Principle of trilateration*

Multi-lateration is the last lateration method. It is based on the difference in distances. Most commonly the multi-lateration techniques is used with time difference of arrival (TDoA). Where the trilateration is distances, which can be seen as circles that intersects, the multi-lateration creates hyperboloids that intersects, due to the distance estimated on time differences, instead of actual ToA measurements. The principle of multi-lateration hyperboloids are found on fig. 2.6.

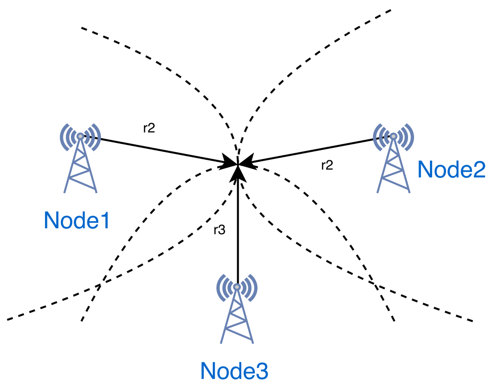

Figure 2.6: *The hyperboloids formed by multi-lateration.*

2.2.3 Scene analysis

The last category for localisation determination is the use of scene analysis. The method of scene analysis is the most common based on a preinstalled system, such as WiFi. The approach is based on creating a map of fingerprints in an offline phase or setup phase. The after initial setup the system in an online phase, uses new measurements to match with the fingerprints made in the offline phase. The fingerprints with the best match for the new measurement is reported as the tag position.

Depending on the accuracy wanted, the fingerprints has to be measured in a equal or finer grid, than the accuracy wanted. This could also be achieved by interpolation the measurements between grid points. The fingerprints measured can be different characteristics of a signal [3], however mostly received signal strength indicator (RSSI) is used. The fingerprints are stored on a server ready for use with different scene analysis algorithms. A downside on the usage of scene analysis is that the offline phase can be time consuming depending on the installation area. Also the scene analysis, depending on algorithm, can also be vulnerable to changes in environment, such as rebuilding a wall or relocating of furnitures/offices or generally movement and changes in environment. Figure 2.7 shows a grid which indicates reference points measured, the grid size can be changed depending on the accuracy. Large grid size(left) gives less accuracy, small grid size (bottom-middle) grants possibility for higher accuracy.

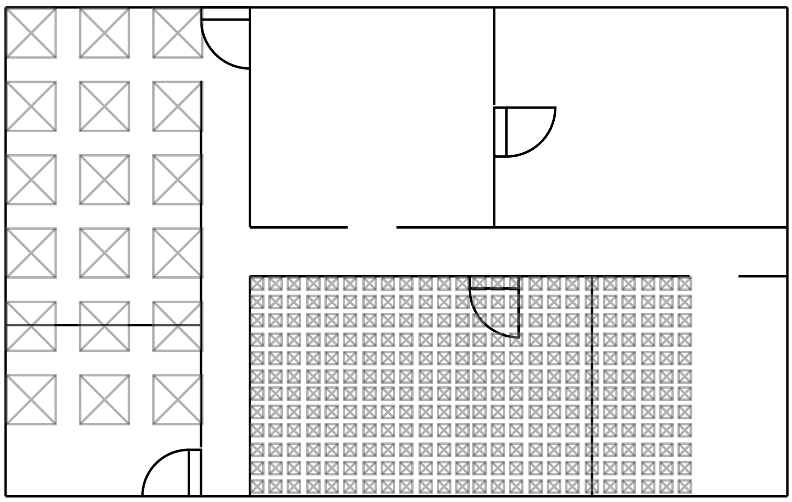

Figure 2.7: *Grid for offline phase of scene analysis, each cross is a measurement point.*

The scene analysis method have the offline approach of measuring reference points, however different methods can be utilised for the online phase to make the fingerprint matching. The online phase is when system has been calibrated and is ready to position devices. From [3] the following algorithms are examined: probabilistic method, k-Nearest Neighbour (kNN) and Machine learning/neural networks.

Probabilistic method considers the probability that given an observed signal strength, s, the position of the tag is located in location L_i. A decision rule is made in the offline phase for creating the fingerprinting map, stating that location, L_i is chosen if:

$$P(L_i|s) > P(L_j|s), \text{ where } j, i = 1, 2, 3.....n \tag{2.1}$$

where n is the amount of locations. Therefore measuring s, the tag position is reported as the position L which obtains highest probability.

Nearest neighbour algorithms is a method used for classification, which assigns a data point to its nearest neighbour or nearest class. Therefore increasing the complexity of the nearest neighbour algorithm increases the probability that the data point is assigned to its right position or class. Following is a description of the nearest neighbour algorithms used in [6]. The estimated position is denoted $\hat{p}$.

NN: is the assignment of $\hat{p}$ as the location of the node with the nearest matching RSSI value(like proximity detection).

KNN: is the comparison of the measured RSSI value with the k-nearest neighbour, where k is a pre-set amount of nodes to compare with. After determining the k-nearest neighbour the average of those points are determined.

WKNN: is the same principle as KNN, but instead of just an average each neighbour point is weighted by a factor which is determined depending on the usage of the system. However for a positioning system using the RSSI value to weighting the different neighbours seems suitable. Thereby the position estimate is found as in eq. (2.2):

$$\hat{p} = \frac{\frac{1}{G_1}L_1 + \frac{1}{G_2}L_2 + \frac{1}{G_k}L_k}{\frac{1}{G_1} + \frac{1}{G_2} + \frac{1}{G_k}} \tag{2.2}$$

where G_k denotes the k'th weighting factor of the different nodes and L_k denotes the location of the k'th node.

EWKNN: is same approach as the WKNN but with an enhancing in the way that k is determined dynamically. This is found to be a better approach for the WKNN, as often when k is static(WKNN), some nodes has a tendency to be at a farther distance, thereby increasing the error when used for estimation, even when weighted. The determination of k in EWKNN is found in [6].

Neural networks can be trained in the offline stage, with a set of reference RSSI measurements and corresponding known locations of tag. The neural networks adopts the input data and calculates a set of weights that is used within a hidden layer in a multi-layer perceptron (MLP) network with a single hidden layer. The output from a neural network will be a 2D or 3D vector holding the estimated position coordinates. For more information of performance, implementation and evaluation, see [7].

Using a neural network to increase the position estimate is not only possible for RSSI, other channel characteristics could also be trained to increase the position estimates. A training algorithm could also be implemented on top of e.g. AoA estimation techniques or on top of the ToA estimation techniques to further improve the accuracy and precision. The machine learning systems could even be implemented alongside the ToA and AoA system to learn how to detect/predict ToA.

2.2.4 Summary of Localisation Methods

Implementations of systems can acquire high accuracy and precision, but often requires a lot of calibration and complex algorithms to achieve satisfying accuracy.

The proximity detection method is not suitable for creating an accurate system, as a fine grid of reference nodes are required.

Lateration techniques is simple to implement, as the only needed knowledge is the installation locations of nodes and from these a tag position can be estimated.

The neural networks to create an IPS, from [7], seems to acquire high accuracy and precision at a wide range from 0 m - 100 m. However the offline and training stage is time consuming especially for larger areas. Also the scene analysis techniques are very sensitive to changes in the environment if based on signal strength.

2.1 lists the different localisation methods and their needed input data.

Localisation method	**Input data**	**Comment**
Proximity detection	Connection/RSSI	Accuracy depends on grid size
Triangulation	Angle	Small measurement error in angle results in large error estimate
Trilateration	Distance	Requires time synchronization
Multilateration	Distance	Requires time synchronization
Probabilistic method	RSSI	High setup cost/time, accuracy depends on grid size
kNN	RSSI	High setup cost/time, accuracy depends on grid size
Neural Network	RSSI, ToA, AoA	Requires training data and complex calculations

Table 2.1: *Summary of the different location algorithms mentioned.*

2.3 Obtaining Input Data

The following section will provide an overview of the different wireless channel characteristics which can be utilised to obtain the input-data needed by the different localisation methods. From the channel the following characteristics can be used to obtain input-data for the localisation algorithms: time of arrival, angle of arrival and received signal strength indicator. Other characteristics might also be possible to use, however these are the most common.

2.3.1 ToA

The trilateration and multi lateration requires requires distance as input. A distance can be obtained using the time of arrival, also known as time of flight (ToF). By measuring the time it takes for the signal to travel from a tag to a node the distance can be acquired, as the speed at which a radio wave travels is known to be speed of light (c). Therefore a distance can be calculated as eq. (2.3):

$$d = c \cdot t_{travel} \tag{2.3}$$

Where c is the speed of light (3×10^8 m/s) and time traveled (t_{travel}) is the time traveled from tag to node.

A signal with $t_{travel} = 100 \times 10^{-9}\,\mathrm{s}$ corresponding to a distance as shown in eq. (2.4):

$$d_{ToA} = 3 \times 10^{8}\,\mathrm{m/s} \cdot 100 \times 10^{-9}\,\mathrm{s} = 30\,\mathrm{m} \tag{2.4}$$

A drawback of using ToA is that this requires a synchronization between tag and nodes. A way to overcome this is to use a similar technique, namely the round trip time (RTT) which is a measure of t_{travel} but for a transmission from tag to node and back, see fig. 2.8.

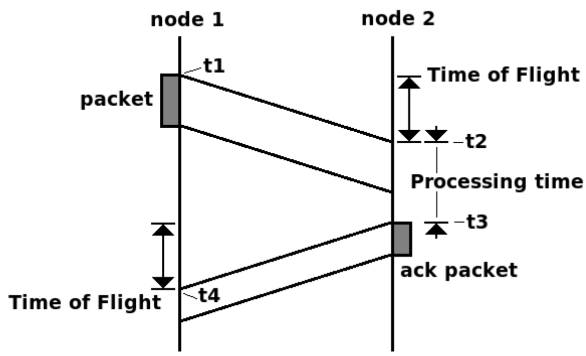

Figure 2.8: *The principle behind the RTT method for distance measurement. Figure from [5].*

The distance can then be calculated using eq. (2.5):

$$d_{RTT} = \frac{(t_4 - t_1) - (t_3 - t_2)}{2} \cdot c \tag{2.5}$$

where $t_3 - t_2$ is the time it takes to process the received signal and transmit it back.

A way to overcome the downsides from ToA and RTT is to use TDoA. From the ToA scheduling between transmission from tag to node is required, and for RTT it is required that the tag is able to both transmit and receive for sending back the signal. Using TDoA the tag and node needs no scheduling, furthermore the tag needs only to be a transmitter, and therefore does not need to be able to receive to be able to calculate a position. This is a result of the system depending on time difference (Δt) instead of absolute travel time, t_{travel}.

Synchronization between nodes now becomes an issue, possibly introducing estimation errors. As a TDoA system is dependent on the time difference, having unsynchronized nodes introduces an estimation error. Two nodes reporting times/distances and being out of sync by $1 \times 10^{-9}\,\mathrm{s}$, using eq. (2.3), results in eq. (2.6):

$$d_{sync-error} = 1 \times 10^{-9}\,\mathrm{s} \cdot 3 \times 10^{8}\,\mathrm{m/s} = 0.3\,\mathrm{m} \tag{2.6}$$

where d_{err} is the introduced distance error due to unsynchronized nodes.

2.3.2 AoA

The triangulation algorithm requires angles as input for locating a tag. An angle can be found using the AoA of a received signal. The most common method to acquire the angle of arrival is to use a linear antenna array. At least two antennas is needed to estimate the angle, however increasing antenna amount increases the accuracy of the estimate. The angles is estimated from the difference in time between reception of a signal at two array elements, with known spacing. The principle is shown on fig. 2.9.

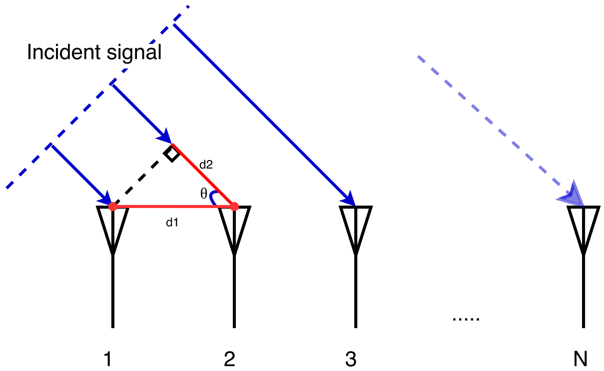

Figure 2.9: *Antenna array used to estimate the angle, θ, at which a signal arrives.*

By knowing the spacing between antenna elements, $d1$ and estimating the distance, $d2$, using Δt and c, the θ can be calculated using trigonometric relations. The linear array can be utilised for determining angle for both static and moving objects.

2.3.3 RSSI

The last input data is RSSI, which can be utilised by two different categories, those being a fingerprint database for the scene analysis and used as a distance measure for the trilateration technique.

The scene analysis methods (Probabilistic method, kNN, Neural Network) all need some kind of calibration/training data in the offline stage, therefore measuring the signal strength in a grid as seen on fig. 2.7, can be used to calibrate the system or as a training sequence with known RSSI values and corresponding locations.

RSSI values can also be used to calculate a distance from tag to node. By knowing the transmitted power and measuring the received power, the power lost through the traveled path can be used to estimate the distance. For simplicity using Friis freespace model for path loss a received power can be converted into a distance using eq. (2.7) assuming a transmitted power is known, in this case 0 dB.

$$d_{fs} = 10^{\frac{(PL - 20log_{10}(f) + 27.55)}{20}} \tag{2.7}$$

where PL is the path loss, f is the frequency in MHz and d_{fs} is distance in free space in meters. 27.55 is a constant given due to the units for the frequency and distance. PL is defined as the difference between transmitted and received power. Figure showing distance as function of path loss is found on fig. 2.10 assuming a transmission power of 0 dB.

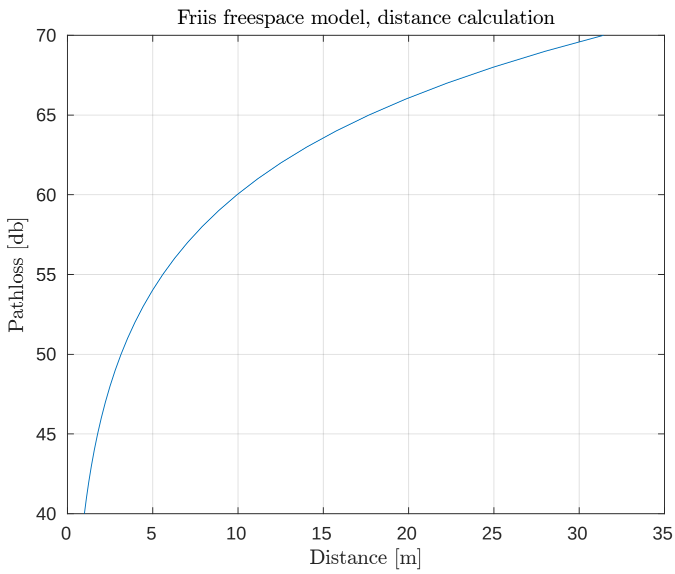

Figure 2.10: *Path loss dependent on distance.*

2.4 Performance Measure

The following section will describe the performance measure for an IPS. The estimation error will is depending on input-data. The first being the euclidean distance measured from the position estimate, $\hat{p}$ to the actual true position, p. We define the error as the Position determination error (PDE) and given a two dimensional plane (x,y) with $\hat{p} = (\hat{p}_1, \hat{p}_2)$ and $p = (p_1, p_2)$, the PDE can be calculated as eq. (2.8):

$$PDE = \sqrt{(p_1 - \hat{p}_1)^2 + (p_2 - \hat{p}_2)^2} \tag{2.8}$$

The second measure is used for the algorithms using distance as input, this is the error estimated in a single distance measurement (three required for position estimate). As this can be utilised to see if different algorithms have a bias in the distance estimate, e.g. if a input-data method is biased towards estimating a longer distance than the actual distance. Therefore is, similarly to positions, introduced a true distance (d), distance estimate ($\hat{d}$), and a distance determination error (DDE).

$$DDE = \hat{d} - d \tag{2.9}$$

Both PDE and DDE are measures of accuracy, however the precision mentioned earlier is also very important. The precision is described by the distribution of either the PDE

or DDE. For the following chapters, the precision will either be described in terms of the distribution of the error source, or by the distribution of simulated or measured errors in DDE or PDE.

In practice, the impact of the environment can introduce large variations on the DDE and PDE. Both AoA, ToA and RSSI has large variations in the indoor environment and chapter 3 evaluates the performance of the different characteristics to find a target for further examination and evaluations.

Chapter 3

Simulations of Basic Localisation Methods

The following chapter will describe the evaluation of the basic channel characteristics and the corresponding methods which can be utilised for position determination. Simulations will be made dependent on the fluctuations, attenuations and other system performance metrics, which impacts the system. The performance metrics is depending on the method investigated.

For some of the localisation methods, especially scene analysis, inspiration and evaluation results were sought elsewhere.

The following sections will provide simple position estimations based on the different localisation methods and channel characteristics mentioned in sections 2.2 and 2.3. Section 3.1 will investigate AoA used with triangulation, where the largest error occurs due to the wide angular spread of the received signal. Section 3.2 examines the usage of RSSI, first in the case of fingerprinting and later as a measure of distance. The largest error here occurs due to fluctuations in RSSI. Following in section 3.3 will be an examination of ToA and the performance of this. The largest error occurs due to the bandwidth of the system and detectability of the direct path. Section 3.4 concludes the basic simulations and summarize the results.

The reason to investigate the basic localisation systems and the performance of these is to find the most promising technique to further investigate for indoor localisation. Therefore no complex or advanced assumptions or algorithms are made for the following evaluations.

3.1 AoA

Examining the angle of arrival for an IPS is a difficult task, as reality shows an AoA which is uniformly distributed in angle between $[0;2\pi]$. This is a result of the reflection on surfaces in e.g. an office. Reflections are made on walls, floors, ceilings, desks, chairs, doors, etc. A raytracing sketch is found on fig. 3.1.

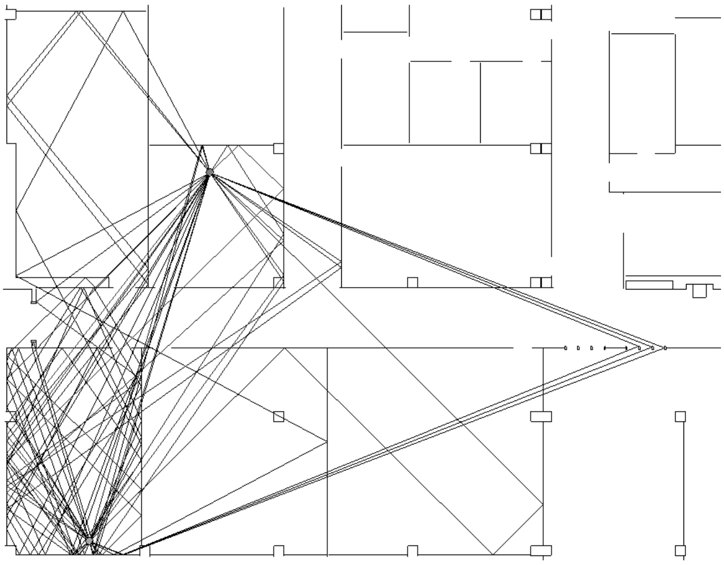

Figure 3.1: *Sketch of an example of isotropic radiating transmitter and the reception at the receiver. Figure from [8].*

Trying to estimate the position of a receiver is impossible with only the AoA if no directivity can be derived from the angular distribution. From [9] it is found that the arrival of direct and reflected paths can be modelled as clusters. As the signal arrives in clusters, it is determined that so does the angle, meaning each cluster has its own angular distribution, see fig. 3.2.

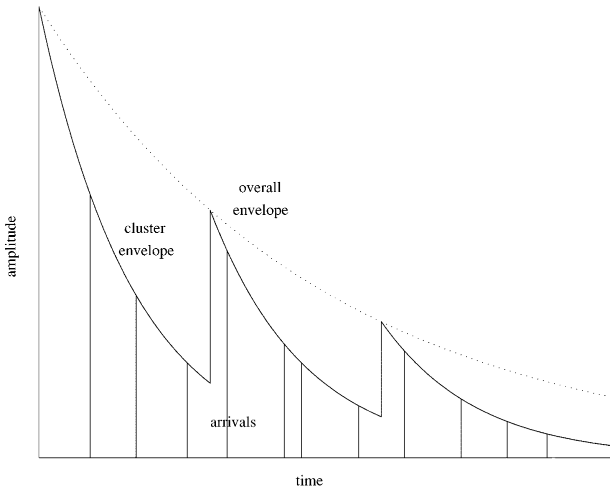

Figure 3.2: *The arrival of a single transmitted signal, with respect to delay. Denoted $h(\tau)$. Figure from [9].*

Measurements carried out suggest clusters arriving at a stationary node having laplacian distribution. The Laplace distribution PDF is defined as eq. (3.1). [9]

$$L(x|\mu, \sigma_\theta) = \frac{1}{\sqrt{2}\sigma_\theta} \cdot e^{-|\sqrt{2}\cdot(x-\mu)/\sigma_\theta|} \tag{3.1}$$

where μ_θ is the mean angle and σ_θ is the standard deviation of the angle. From [8, 9] surveying the indoor environment with regards to AoA, the laplacian distribution is found to have the best fit for σ_θ distributed between 22-26°. The distribution created using eq. (3.1) is shown on fig. 3.3.

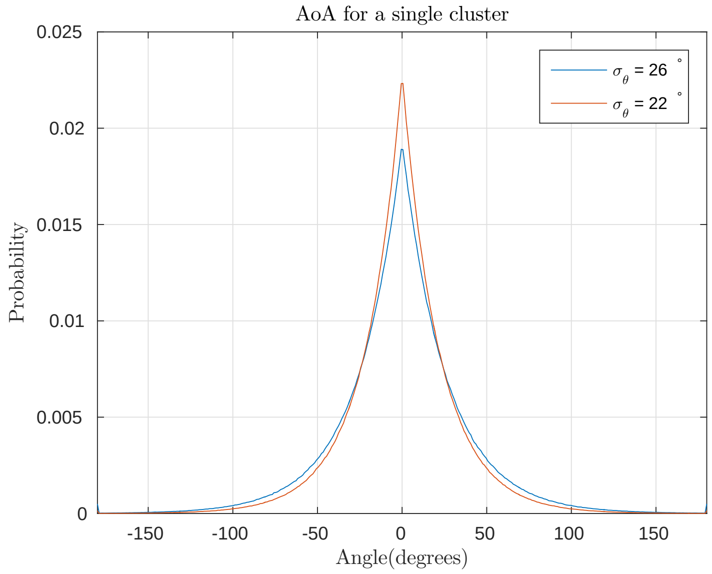

Figure 3.3: *AoA distribution modelled as a laplacian distribution with μ_θ = 0 and σ_θ = 22-26°.*

As mentioned the general mean angles are distributed $U[0, 2\pi]$, but if the signal arrives with a detectable direct path, it is assumed possible to identify the AoA for the first cluster. For triangulation at least 2 nodes are needed, also it should be possible to identify the first cluster at each node.

A system based on AoA have an accuracy which is dependent on the amount of nodes installed, this is due to the accuracy being a function of the distance from tag to node. It is a known that a small change in angle at the node, corresponds with a large change of position estimate far from the node. Therefore dense deployment of nodes or accurate AoA measurements is required.

AoA has been evaluated with the following assuptions, see table 3.1.

Node and tag position distribution in X and Y	U(0,35)
Angular receiption distibution	L(μ_θ,σ_θ)
μ_θ	0°
σ_θ	$22 - 26°$
Tag amount	1
Node amount	3

Table 3.1: *Assumptions used for simulations.*

Figures 3.4a and 3.4b show best and worst case for amount of intersections with 3 nodes and 1 tag, it is assumed that the 3 nodes can not be placed within 5 m of each other.

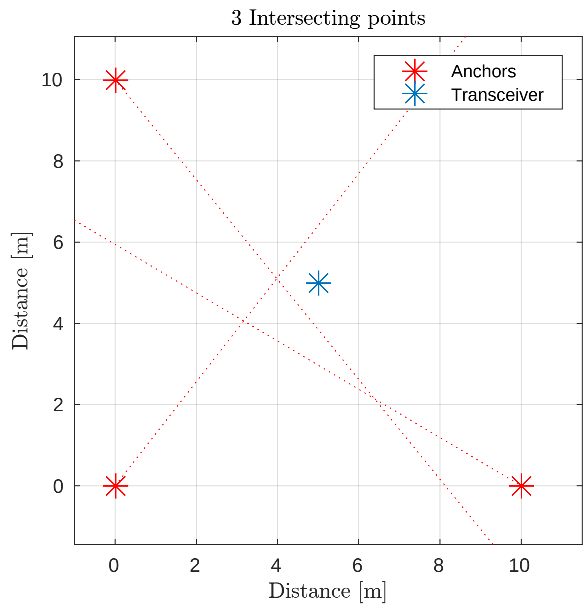

(a) *Best case.*

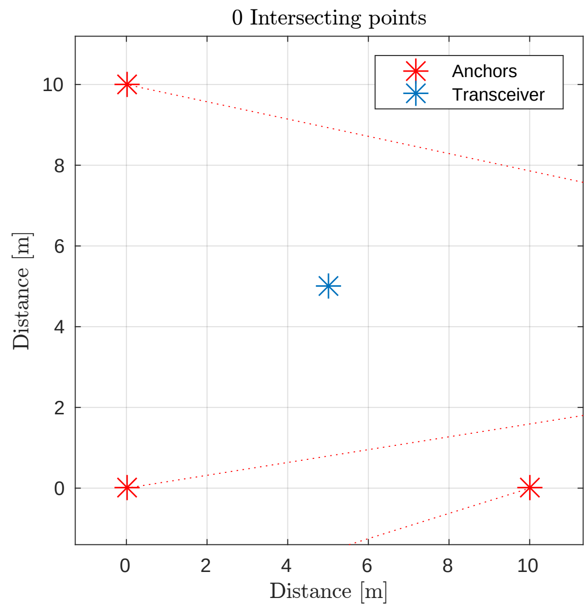

(b) *Worst case.*

Figure 3.4: *Best and worst case scenario for intersecting points. Transceiver is location of the tag.*

A set of measurements is simulated, redistributing the nodes and tag and calculating the intersecting points. Further the algorithms in figs. 3.5a and 3.5b is used for evaluation.

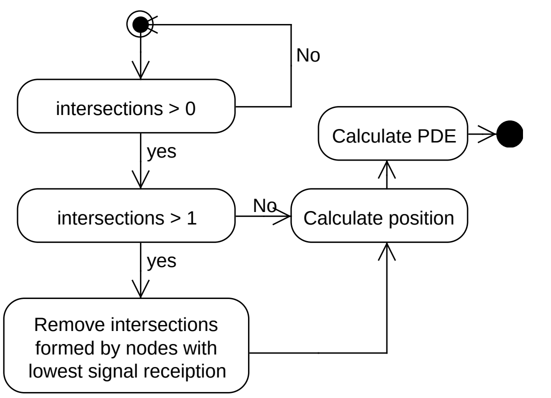

(a) *Neglecting algorithm based solely on 1 intersection point.*

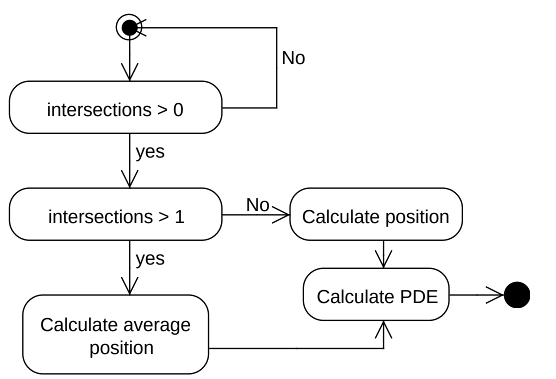

(b) *Algorithm calculating the average of intersection points.*

Figure 3.5: *Algorithms used for evaluating AoA.*

The resulting PDE is plotted as a cumulative distribution function (CDF) found on fig. 3.6. It is seen that the averaging algorithm achieves a more accurate estimate, however the errors are still ranging from 5 m - 7.5 m at the 50 percentile level. and errors as large as 13 m - 17 m is achieved at the 90 percentile level.

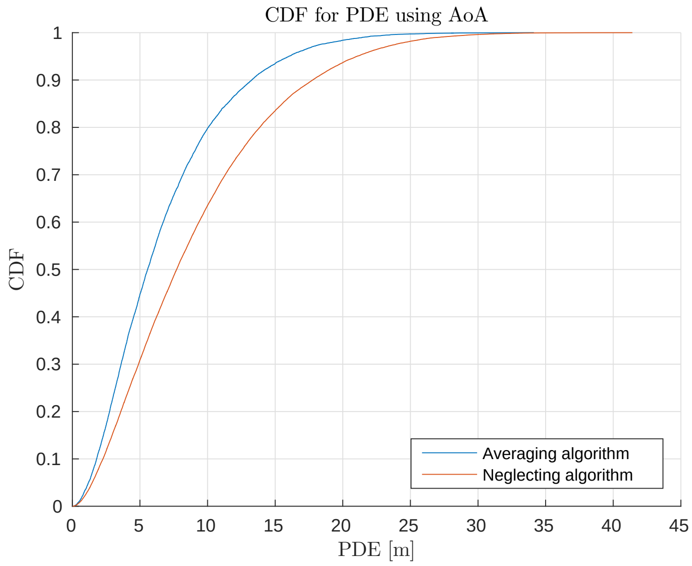

Figure 3.6: *CDF for PDE using AoA.*

3.1.1 Conclusion of AoA

Summarising the usage of AoA as input data to a triangulation algorithm it can be seen that the system is inaccurate, with a mean error of 5-7.5 m. The main problem with AoA is first of all the large angular spread, but also the ability to detect the first arriving peak. If the first peak is undetected this introduces large errors (or no position at all).

3.2 RSSI

The following section will investigate the use of signal strength to create an IPS.

First is the usage in a fingerprinting system. A fingerprinting system creates a lookup table depending on different RSSI values from anchor nodes, then when a position is wanted a measurement is made and matched with the lookup table. The lookup could either be based on a simple statistical method, or by the usage of neural networks to train data as mentioned in section 2.3.3. The results here is found in other literature.

Second is a propagation method, where a path loss model is calibrated to match the given environment. Then a transmission from a tag is made, and the RSSI from a set of nodes is translated into a distance and through lateration the position of the tag is estimated.

3.2.1 Fingerprinting

For the accuracy of a fingerprinting system, inspiration and results in other literature has been found, as implementation and testing of such system would require much time, also the precision of fingerprinting systems differs a lot depending on the individual system and setup area.

Examining the fingerprinting based method, the accuracy in these systems depends mostly on the amount of nodes and the resolution of the fingerprinting grid, together with the fingerprinting algorithm.

The different positioning algorithm has been analysed with regards to performance, this is shown in fig. 3.7a. Figure 3.7b shows how the changes to distance between grid points changes the accuracy of the PDE. The evaluations are made in a 48 m x 22 m area with static preinstalled nodes. [6]

The examined algorithms are NN(Nearest neighbour), KNN(k-nearest neighbour), WKNN(weighted k-nearest neighbour) and EWKNN(enhanced weighted k-nearest neighbour), the algorithms are described in fig. 2.7. Using the more advanced algorithms increases the accuracy of the system, a KNN algorithm implemented in the system gives 2 m accuracy with a 45% confidence level, however for a EWKNN the 2 m accuracy is given with a 60% confidence. [6]

It seems to be a general improvement of 15% confidence changing the algorithm from NN to EKWNN.

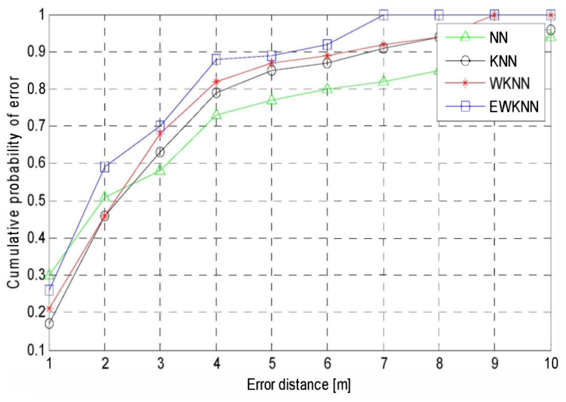

(a) *The CDF for distance error using different algorithms in a fingerprinting system.*

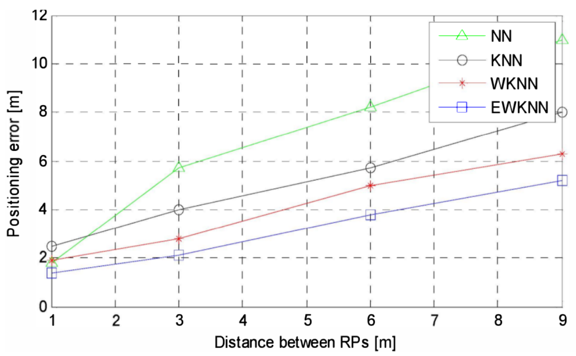

(b) *The impact of the spacing between grid points for different algorithms.*

Figure 3.7: *Impact of spacing and the CDF for distance error in fingerprinting system. Figures from [6].*

Assuming the usage of a fingerprinting system is navigation or tracking of moving objects or persons, changes in the environment occurs as people moves around. As a result of this, even though the system is calibrated at each reference point, a fading due to shadowing would affect the systems position estimates.

3.2.2 Distance Propagation Method

In the following section the accuracy of a distance propagation method will be investigated. Generally a propagation based method is inaccurate compared with a fingerprinting system, which often is a result of shadow fading in an indoor environment. The impact of the shadow effects are lowered in a fingerprinting system as the calibration procedure takes into account the attenuation of walls, roofs and other stationary attenuating objects.

The RSSI at a node corresponds with a distance due to the path loss as function of distance as seen on fig. 3.8. Using Friis freespace model for calculating the corresponding distance, measuring a RSSI of -60.5 dBm equals a distance of 10 m and -66.07 equals 20 m, see fig. 2.10 and eq. (2.7). The simple freespace model does however not match the attenuation introduced in an indoor environment and therefore the LNSM(Log-Normal Shadow Model) is often utilised instead, as this is a better match compared with experimental data and also includes a probabilistic variation of the shadow effect. From [10] the LNSM model is described as in eq. (3.2).

$$PL(d) = PL(d_0) + 10\eta log_{10}(\frac{d}{d_0}) + X \tag{3.2}$$

Where d_0 is the near-earth reference distance, η is the path loss index often between 2-5 and X_σ is a zero mean gaussian random variable, with σ_X being standard deviation between 2-8 dB from [10, 11]. Assuming no variation in the model($X_\sigma = 0$), the distance become deterministic and the resulting propagation model is plotted in fig. 3.8 with $\eta = 3$ and $PL(d_0) = 41$ which is experimental values from [10]. It seen that the LNSM which represents experimental values has a higher path loss. The LNSM will be used for further calculations in this section, as it is assumed that this model better represent the actual attenuation of a signal in an indoor environment. For a real life implementation of a distance propagation system, it would require a fitting of a path loss model with the environment that it is going to be deployed in.

Taking the variations of the LNSM into consideration the signal with variation can be found on figs. 3.9a and 3.9b. Due to the fluctuation of the RSSI a distance is no longer deterministic from a single RSSI value but is now ambiguous, e.g. -70 dB ranges from a distance between 1 m and 40 m in the case that σ_X equals 6, however for the case that σ_X is 2 the span is approximately 6-13 m.

It is known that for a setup of a IPS system, the nodes would be placed in known positions however with distances in between. Therefore simulations with 3 randomly distributed nodes and a tag is made, which results in a CDF the PDE (position determination error) as seen on fig. 3.10. For the simulations a standard deviation of the shadow fading of 2 dB was used. To compare with simulation results from section 3.1 the node positions are $U(0, 35$ for both X and y direction and restricted to have a minimum distance between them of 5 m.

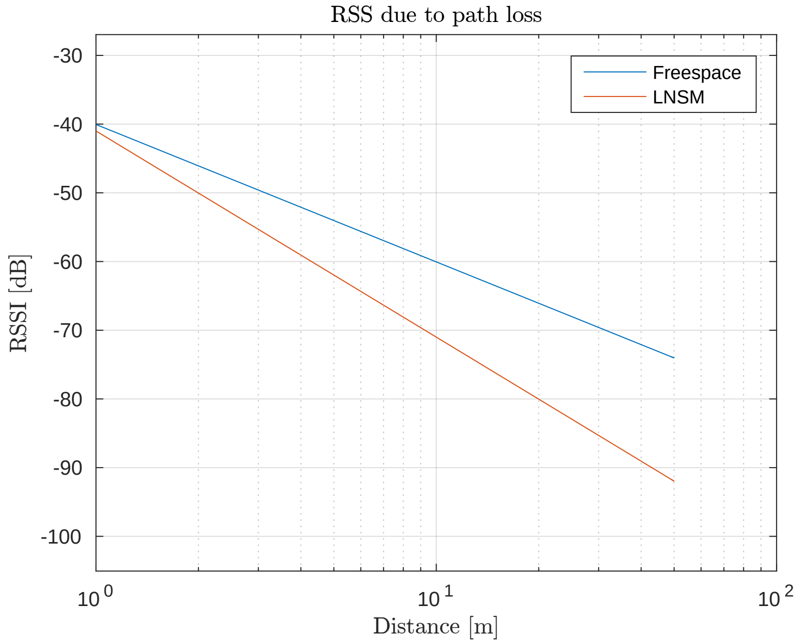

Figure 3.8: *The received RSSI corresponding with distance for free space and LNSM.*

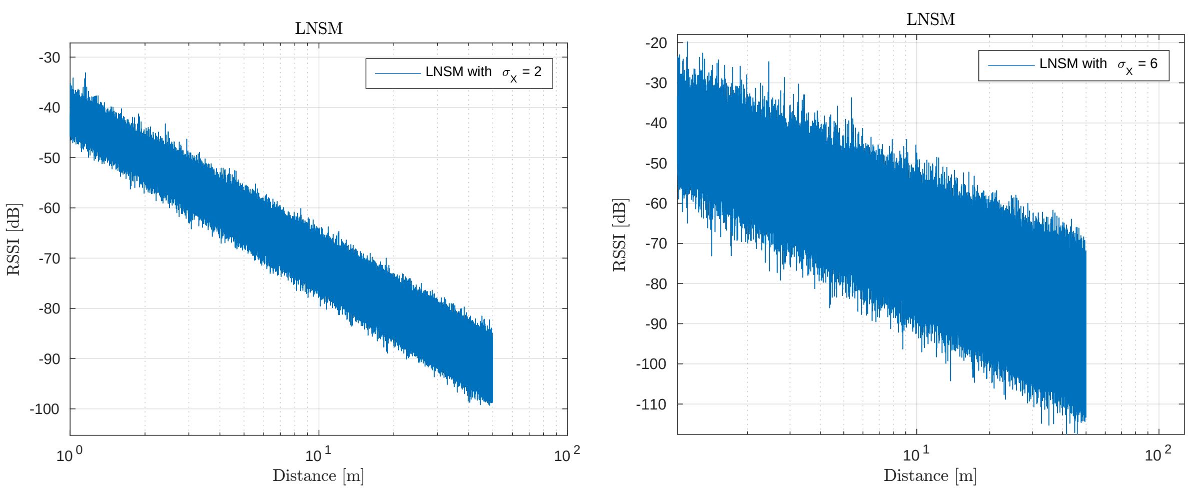

(a) *LNSM with σ_X of 2*

(b) *LNSM with σ_X of 6*

Figure 3.9: *LNSM with shadow fading implemented with different standard deviation.*

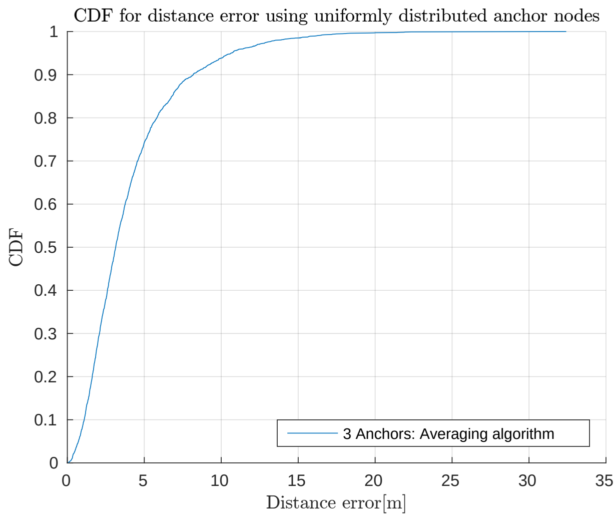

Figure 3.10: *Distance errors for uniform distributed nodes and tag.*

3.2.3 Conclusion of RSSI

For the RSSI systems, the fingerprinting system could be used for smaller areas, however creating a fingerprinting map for e.g. a warehouse or hospital would require a huge offline phase and the variations in these areas are high due to the movement in such places.

For the distance propagation method, the accuracy is better compared with the AoA method. The AoA has an accuracy of 13.5 m with 90% confidence in a 35x35 m area, whereas this has increase to 7.5 m with 90% confidence by using RSSI instead. It should be noted that this is by assumption that the noise fluctuation is low.

3.3 ToA

In the following section the accuracy of ToA also known as ToF examined. Generally a ToA system is not accurate in a multipath environment due to the attenuation of signals and reflections created. The reason for this is often the bandwidth (B) as this is the determining factor for differentiating the direct path signal from the reflected signals. A higher bandwidth of the system increases the time resolution thereby increasing the chance of correct ToA estimation.

A ToA system is generally based solely on the performance of detecting this first peak. The reflecting paths for the purpose of creating ToA is not very important for creating an IPS, only the signals arriving very close to the direct path has impact on the performance.

As the time resolution is given by the bandwidth of the system, this can be described as eq. (3.3):

$$T_{res} = \frac{1}{B} \tag{3.3}$$

Generally in a system estimation of ToA can't be obtained more precise than what is allowed by the system bandwidth.

The reflections can be seen as a set of *sinc*-functions with different time-delays and complex weights, as mentioned in appendix B. It should be noted that the sinc-function occurs when a rectangular window is used to convert the frequency domain data to time domain impulse response. Using a hamming window instead the pulse shape would be a raised cosine, as the sidelobes are suppressed. Having a large bandwidth allows for these pulse shapes to be narrower, thereby allowing for easier differentiation between the different paths. By having $B = \infty$ the pulse shapes converges to a dirac pulses and the exact time-delay can be found.

As $B = \infty$ is not possible to obtain, the received signal will be a sum of the pulses at different time-delays.

It can be seen that the having a system with a high bandwidth will allow for precise ToA estimates whereas creating a ToA IPS system seems like a good solution. For a signal in a LOS scenario the peak is easily detected, see fig. 3.11a. However for a NLOS situation the direct peak can be highly attenuated and might be undetectable, see fig. 3.11b. For the ToA method the undetected direct path will result in an estimation error.

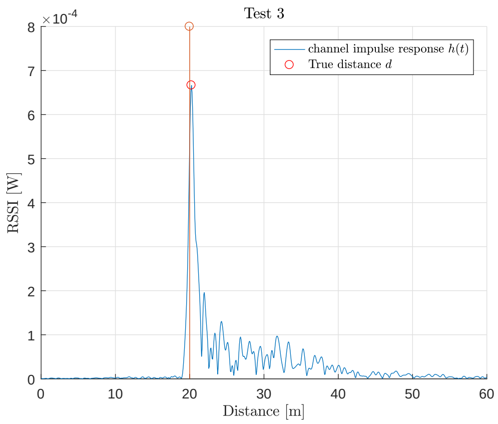

(a) *Channel impulse response for Test 3.*

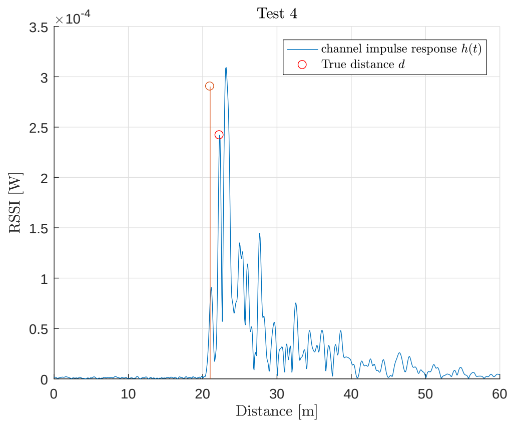

(b) *Channel impulse response for Test 4.*

Figure 3.11: *Measured wireless channel for LOS and NLOS condition. $B = 1GHz$. X-axis are converted from time to distance through eq.* (2.3)*. The channel responses are measured in appendix A.*

As mentioned lowering the bandwidth make it harder to detect the different peaks. fig. 3.11b and fig. 3.11a are wireless channels as seen with $B = 1\,\text{GHz}$ and the direct paths for the LOS case is easily detected. The same wireless channels as seen with a bandwidth of $B = 40\,\text{MHz}$ is found on figs. 3.12a and 3.12b. As it can be seen, even though peaks are found, in a lower bandwidth system the first peak doesn't necessarily correspond with the true ToA, and large estimation errors can be introduced.

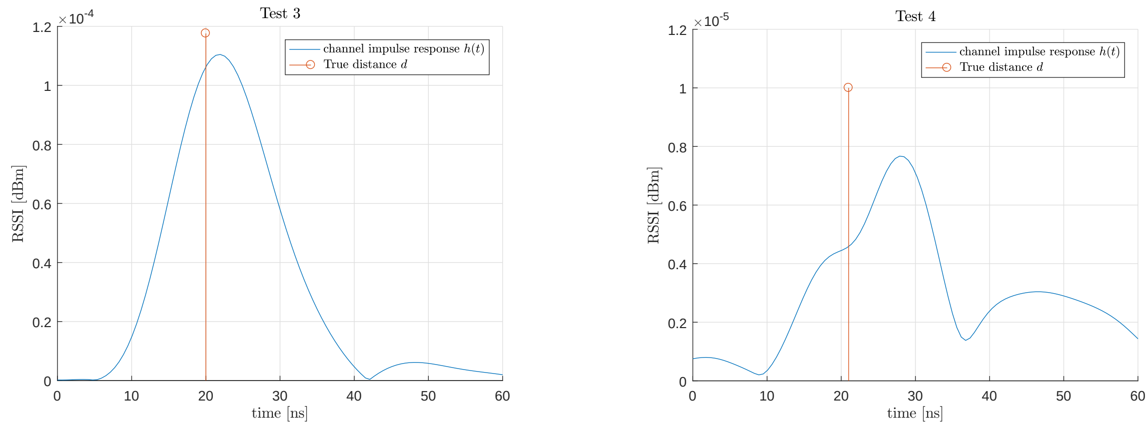

(a) *Channel impulse response for Test 3.* **(b)** *Channel impulse response for Test 4.*

Figure 3.12: *Measured wireless channel for LOS and NLOS condition. $B = 40MHz$. X-axis are converted from time to distance through eq.* (2.3)*. The channel responses are measured in appendix A.*

3.4 Conclusion of Basic Localisation methods

To summarize the evaluation of the basic localisation systems different methods has been tested. The AoA does not seem to achieve satisfying accuracy for an IPS. The evaluations made shows accuracies of 5-7.5 m, however this has been tested with a detectable direct path. For an undetectable path, the accuracy would be even worse.

For the RSSI the performance of the fingerprinting technique seems to obtain suitable performance. However the calibration and setup cost and time does not seem to fit the purpose of installing an IPS in larger areas.

RSSI used for measuring distance could be used with an averaging of several uncorrelated measurements as this would help combat the fluctuations from the wireless channels and therefore achieve better accuracy.

Using ToA as a measure of distance to an object seems to be the most suitable option, as a system implemented with a high bandwidth could achieve rather accurate and precise estimates of the ToA. The largest error in a ToA system occurs when the direct path is attenuated below receiver sensitivity, as this results in an estimation error.

For further investigation the ToA method will be examined and the impact of bandwidth and a more complex computation methods will be utilised to further improve performance.

Chapter 4

ToA Positioning with Time Resolution Enhancement

The following chapter will describe the investigation of a more complex ToA algorithm to further improve the ToA detection when using lower bandwidth systems. This is a result of the ToA concluded the most promising technique in chapter 3.

From the further investigation of enhancing the ToA system, it is seen in several articles [12–15], that the eigenvalue decomposition (EVD) method seems like a good candidate for developing a high-accuracy IPS. EVD is utilised in a set of different algorithms, from these the MUltiple SIgnal Classification (MUSIC) algorithm is used.

The chapter will consist of two parts, in sections 4.1 to 4.6 is a description of a system model for a transmitter and receiver system. Following in section 4.7 is a description of the MUSIC algorithm.

4.1 I/Q baseband description

The system will only be described using the equivalent baseband signal. For describing a transmitted sequence such as data or pseudo random noise (PRN) the signal can be described by its amplitude and phase or by the baseband signal in terms of the mathematical representation of I/Q. I and Q are respectively the in-phase and quadrature component of a signal.

The structure of the I/Q baseband signal can be found from the amplitude and phase of the signals as found on fig. 4.1.

Using simple trigonometric properties, the following equations can be constructed:

$$A = \sqrt{|I^2 + Q^2|} \tag{4.1}$$

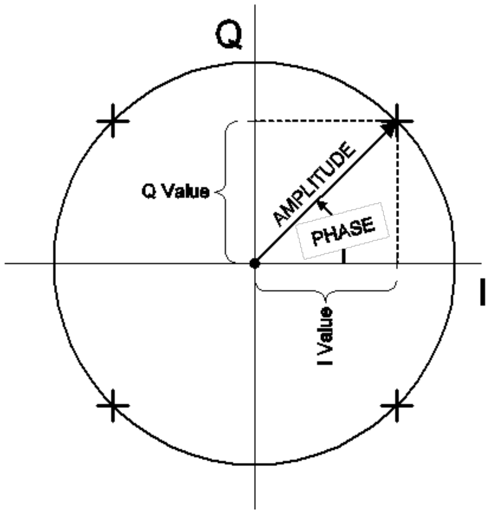

Figure 4.1: *Baseband signal representation setup. Picture from [16].*

$$\phi = tan^{-1}(Q/I) \tag{4.2}$$

$$I = A \cdot cos(\phi) \tag{4.3}$$

$$Q = A \cdot sin(\phi) \tag{4.4}$$

where A is amplitude and ϕ is phase.

Using Eulers form we can write the I and Q signals into a plain signal using $cos(\phi) + j \cdot sin(\phi) = e^{j \cdot \phi}$ we can write the complex signal $I + jQ$ as:

$$I + jQ = A \cdot e^{j \cdot \phi} \tag{4.5}$$

Section 4.4 explains how the I and Q terms can be used to transmit a BPSK modulated signal.

4.2 System Model

The overall block diagram describing the transmitter/receiver system for implementation of a MUSIC algorithm is found on fig. 4.2. The yellow marked blocks are not described, Therefore only the equivalent baseband signal will be described together with the impact of the wireless channel and the changes introduced by the passband filters in the down-conversion. Therefore the errors introduced in the RF modulator and demodulator will not be taken into further consideration.

The "MUSIC algorithm" block is a larger block and is further described in section 4.7.

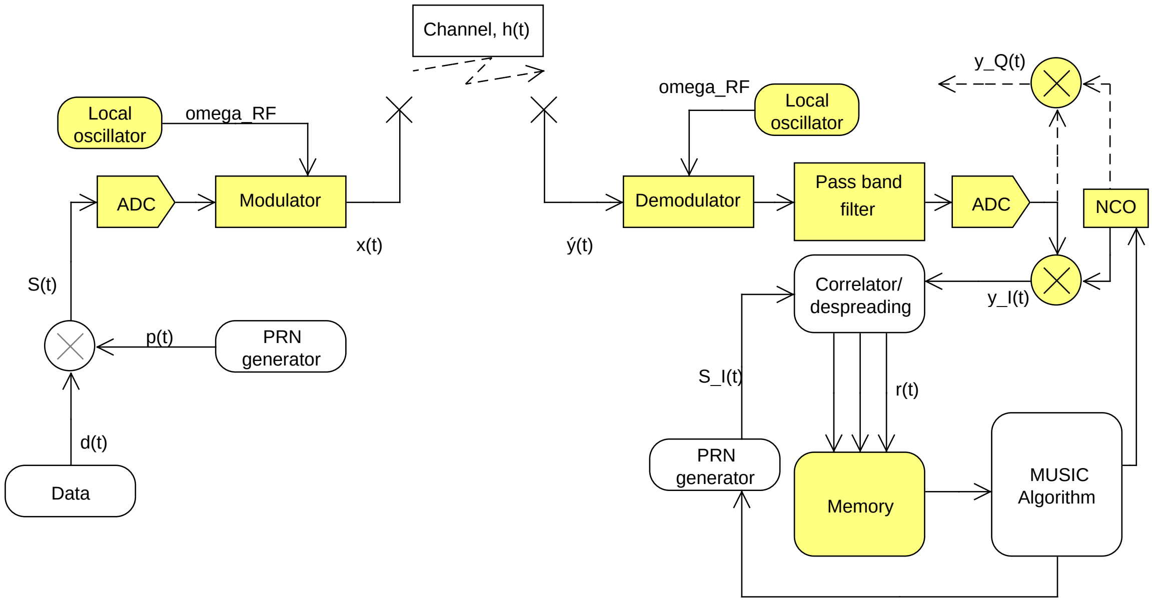

Figure 4.2: *Block diagram for overall IPS system with data acquisition and calculations. Yellow blocks are not described in this thesis.*

4.3 Identification data

Assuming that several tags are used for locating several different objects, it is important to be capable of differentiating the tags from each other so that identifying the tag is possible.

To identify which tag is communicating its position, ID data is transmitted as part of the transmission sequence. The ID data could also include other measures such as temperature, pressure or similar.

The data sequence will be denoted $d(t)$ and described as:

$$d(t) \qquad for\ t \leq T_d \tag{4.6}$$

where T_d is the duration of the data for transmission. The data sequence $d(t)$ will be used together with the PRN sequence to transmit the ID data, obtaining processing gain and detecting the ToA of the system.

The Galileo GPS the system generates $d(t)$ with 50 bits/s and the PRN sequence with 1.023.000 chips/s. For GPS the PRN sequence $p(t)$ is 1023 chips. Transmitting 1 data bit from $d(t)$ is it required to transmit 20 PRN sequences as $\frac{T_d}{T_s} = 20$. where T_s is transmission time of a PRN sequence.

4.4 Gold Code PRN Sequence

For transmitting the data $d(t)$ and to obtain an estimate of the wireless channel a PRN sequence is utilised for making direct sequence spread spectrum (DSSS) transmission.

The idea is to transmit the data $d(t)$ with a given bandwidth B_d over a much larger bandwidth B_p given by the PRN sequence $p(t)$. This introduces a so called spreading/processing gain, G_P, which allows for longer transmission ranges compared with just transmission of the data directly onto the carrier.

$$G_P = \frac{B_p}{B_d} \tag{4.7}$$

where B_p is the bandwidth of the PRN sequence and B_d is the bandwidth of the ID data [17].

The PRN code $p(t)$ can be seen as a sequence of chips $c(t)$.

$c(t)$ is defined as eq. (4.8):

$$c(t) = \begin{cases} 1, & \text{for } -T_c/2 < t < T_c/2\,, \\ 0, & \text{Otherwise} \end{cases} \tag{4.8}$$

where T_C is duration of a single chip.

Using the chip time $c(t)$, the PRN sequence $p(t)$ is given by eq. (4.9)

$$p(t) = \sum_{i=0}^{N} c(t - i \cdot T_c - T_c/2) \qquad \text{for } 0 < t < T_s \tag{4.9}$$

Where $T_S = N \cdot T_c$ and N is amount of chips.

$p(t)$ is the PRN code used to make DSSS on the data signal, $d(t)$. The method for combining the data with the PRN sequence is XOR'ing the bits as seen on fig. 4.3. The spreaded sequence will be denoted $S(t)$.

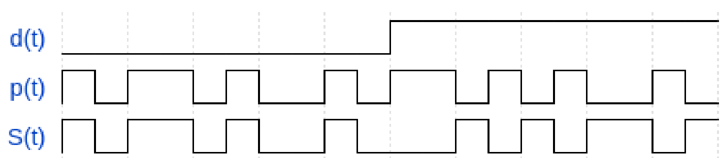

Figure 4.3: *Combining of $d(t)$ and $p(t)$ to make $S(t)$.*

The sequence $S(t)$ is transmitted over the wireless channel using BPSK. Represented as a baseband signal where the phase, ϕ, of the transmitted signal is $[0, \pi]$ to represent the bits 0 and 1. For $\phi = [0, \pi]$ the baseband signal can be represented using only the inphase term, I, as the Q term using eq. (4.4) equals zero.

The transmitted baseband signal can be found on fig. 4.4, assuming an amplitude $A = 1$.

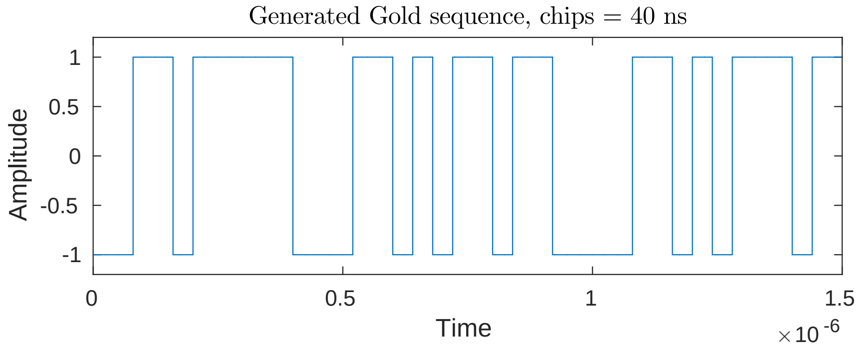

Figure 4.4: *Generated gold code sequence.*

The ID data is not the important factor, the PRN sequence is what is utilised for obtaining a better ToA estimate. Therefore further analysis of $S(T)$ will not be performed and only the PRN sequence $p(t)$will be analysed further.

For the PRN sequence $p(t)$ a Gold Code is utilised, the reason for this is the unique properties held by this specific code, namely a sharp autocorrelation and very low cross correlation with other PRN codes.

The autocorrelation of the PRN sequence is denoted $R_p(\tau)$ and defined in eq. (4.10):

$$R_p(\tau) = \frac{E[(p(t) - \mu_{p(t)})(p^*(t+\tau) - \mu_{p^*(t-\tau)})]}{\sigma_p \sigma_{p_{t-\tau}}} \tag{4.10}$$

where μ and σ are the respective mean and standard deviation for $p(t)$.

The cross correlation of two independent sequences $p(t)$ and $x(t)$ is denoted $R_{px}(\tau)$ and is given by eq. (4.11):

$$R_{xy}(\tau) = \frac{E[(p(t) - \mu_{p(t)})(x^*(t+\tau) - \mu_{x^*(t-\tau)})]}{\sigma_{pt} \sigma_{x_{t-\tau}}} \tag{4.11}$$

where μ and σ denoted by indexes are the are the respective mean and standard deviation for the distribution.

To generate the PRN sequence a psuedo random noise generator with deterministic combinations is used. The PRN code for Galileo GPS is given by the following equations:

$$P1 = 1 + x^3 + x^{10} \tag{4.12}$$
$$P2 = 1 + x^2 + x^3 + x^6 + x^8 + x^9 + x^{10} \tag{4.13}$$

The polynomials is actually not polynomials, but are indexes to a MLS (maximum length sequence) generators, with register lengths n. The MLS generators generates two independent PRN sequences and by combining those two by XOR'ing, a PRN sequence is generated. The resulting PRN sequence even though deterministic holds the same statistical properties as noise. Which is the high autocorrelation as mentioned earlier and the low cross correlation with other sequences or noise. The generator system is found on fig. 4.5:

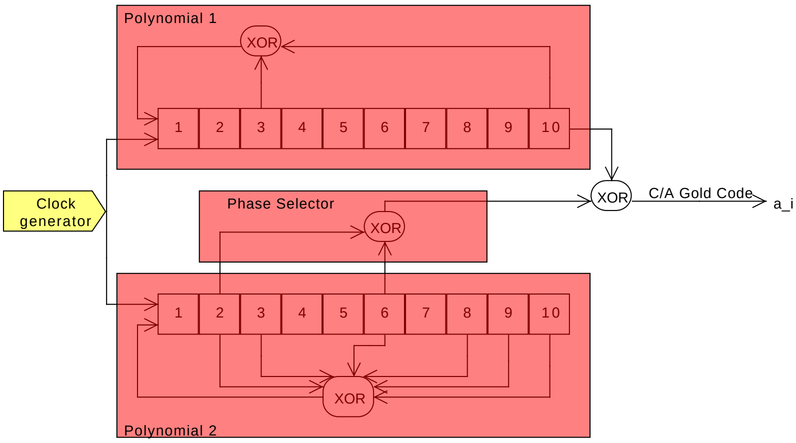

Figure 4.5: *PRN gold sequence generator setup.*

From [17] the maximum correlation of the system is described in terms of the length, N of the generated PRN sequence, the description is given by eq. (4.14).

The maximum autocorrelation for a PRN gold sequence is found at $R_p(0)$ which is the peak of the function. The autocorrelation for a gold code with $n = 10$ will be 1 at $\tau = 0$. The autocorrelation for a PRN gold sequence for $\tau \neq 0$ is $1/N$.

$$R_p(\tau) = \begin{cases} 1, & \text{for } \tau = 0\,, \\ 1/N, & \text{otherwise} \end{cases} \tag{4.14}$$

From [18] the maximum cross correlation between different sequences of Gold Code is described. By choosing the different codes w.r.t. a known boundary the codes can be generated(chosen) with a known maximum cross correlation between sequences.

The maximum cross correlation between two different sequences $p1$ and $p2$, each which are Gold Codes, is given by eq. (4.15)

$$|R_{S1,S2}| \leq \begin{cases} \dfrac{2^{(n+1)/2}+1}{N}, & \text{for } n \text{ odd}, \\ \dfrac{2^{(n+2)/2}+1}{N}, & \text{for } n \text{ even} \end{cases} \tag{4.15}$$

where n is the amount of bits in the MLS generator and N is the total length of the sequence.

Given the Gold code used for GPS satellites, and a MLS generator with $n = 10$, the maximum theoretical cross correlation for two different PRN sequences is:

$$|R_{p1,p2}| \leq \frac{2^{(10+2)/2}+1}{1023} = 65/1023 \approx 0.064 \tag{4.16}$$

The receiver for a system utilising Gold Code searches to maximize the cross correlation between the received signal and a replicated gold code sequence at the receiver node.

For the an implemented Gold code generator the corresponding autocorrelation can be found on, see fig. 4.6.

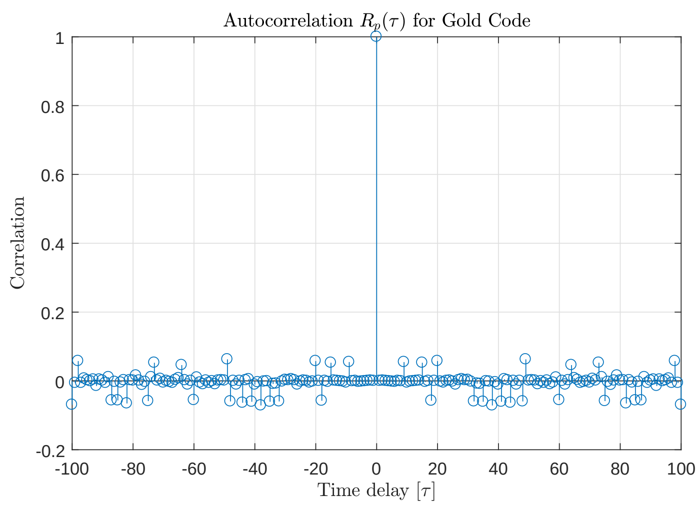

Figure 4.6: *Autocorrelation of the Galileo GPS system (Gold Code).*

As mentioned in eq. (4.14) the maximum correlation is found at $R_p(0) = 1$. The maximum cross correlation for the system, as mentioned in eq. (4.15), is 0.0635 and the maximum autocorrelation value is found to be 0.0625 for the simulations. The reason that the autocorrelation for the system can obtain the values of the cross correlation of a sequence and that sequence delayed can be combined to create a third sequence, which also has the properties of the gold code.

4.5 Channel

The transmitted sequence $p(t)$ is sent over a wireless channel. The wireless channel will be described by the use of a multi path environment model with uncorrelated scatters in both time and frequency domain. The reason for uncorrelated scatters is that each reflected path due to e.g. tables, walls, chairs, windows and similar, are independent. Therefore the channel $h(t)$ can be described as a sum of K paths each path i with its own attenuation α_i, phase shift ϕ_i and time-delay τ_i. The model is described in eq. (4.17):

$$h(t) = \sum_{i=0}^{K-1} \alpha_i \cdot e^{j\phi_i} \delta(t - \tau_i) \tag{4.17}$$

The channel described by its I/Q terms can be seen on eq. (4.18).

$$h(t) = h_I(t) + j \cdot h_Q(t) \tag{4.18}$$

Using the PRN-sequence description from fig. 4.3 with the corresponding I/Q term, the transmission of $p(t)$ over the wireless channel is a complex convolution of $h(t)$ and $p(t)$. Denote the received signal $r(t)$ this can be described by eqs. (4.19) to (4.21):

$$\begin{aligned} r(t) &= p(t) * h(t) + w(t) && (4.19) \\ &= (p_I(t) + j \cdot p_Q(t)) * (h_I(t) + j \cdot h_Q(t)) + w(t) && (4.20) \\ &= p_I(t) * p_I(t) + p_I(t) * j \cdot h_Q(t) + j \cdot p_Q(t) * h_I(t) + p_Q(t) * h_I(t) + w(t) && (4.21) \end{aligned}$$

Where $w(t)$ is additive white gaussion noise (AWGN).

Using the BPSK transmission the quadrature component for $p(t)$ equals zero and the above reduces to eq. (4.22):

$$r(t) = p_I(t) * h(t) + w(t) \tag{4.22}$$

Having a Gold Code as seen on fig. 4.7a convolving this with a wireless channel with only a 40 MHz bandwidth as seen on fig. 4.7b the resulting convolution (received signal $r(t)$) is pictured on fig. 4.8.

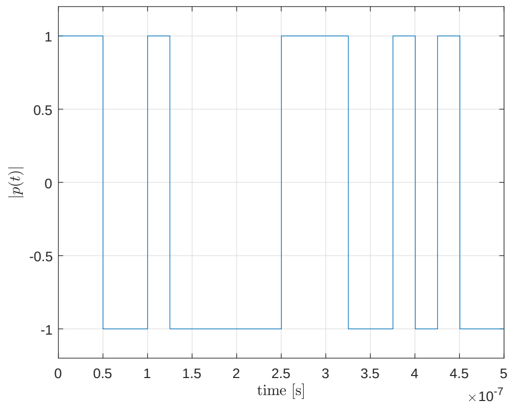

(a) *Realisation of the first few chips of $p(t)$ using Gold Code.*

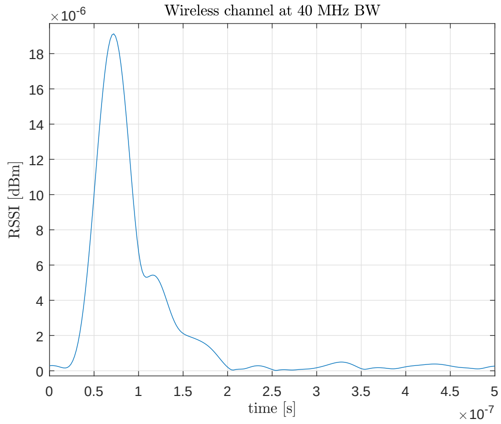

(b) *Wireless Channel with a bandwidth B = 40 MHz. Measurements described in appendix A.*

Figure 4.7: *Realisation of $p(t)$ and $h(t)$.*

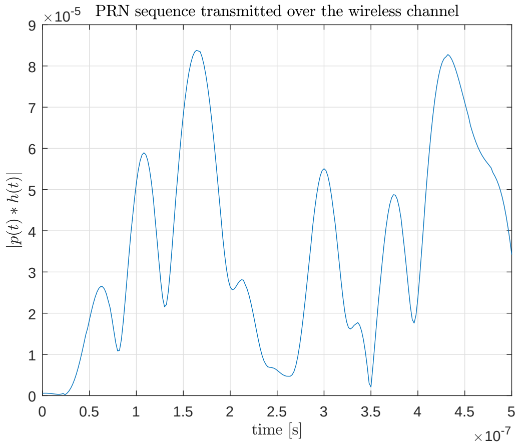

Figure 4.8: *Received signal $r(t)$ obtained by a convolution of $p(t)$ with $h(t)$.*

4.6 Correlator/despreading

After receiving the signal $r(t)$ it is correlated with a replicate of the known PRN sequence $p(t)$. thereby obtaining the correlation properties of the Gold Code, and from the high peaks in the correlation detect the ToA. The autocorrelation properties is described in section 4.4.

As it is known that a convolution with a signal complex conjugated and time reversed is the definition of correlation. Therefore using a convolution of $r(t)$ with $p^*(-t)$ the correlated signal $y(t)$can be expressed as eq. (4.23):

$$y(t) = r(t) * p^*(-t) \tag{4.23}$$

Which can be rewritten as eq. (4.24):

$$y(t) = R_p(\tau) * h(t) + w(t) \tag{4.24}$$

It is now seen that $y(t)$ is expressed as the autocorrelation of the sequence $p(t)$ convolved with $h(t)$. The signal $y(t)$ is shown on fig. 4.9a, this is found by correlating the channel found on fig. 4.8 with a time shifted version of the intial transmitted prn sequence $p(t)$. This is plotted together with the autocorrelation for that specific PRN code $R_p(\tau)$. From fig. 4.9b is is easily seen that the the autocorrelation is time shifted by a delay τ, in this case approximately 75 ns corresponding with a distance of 22.5 m.

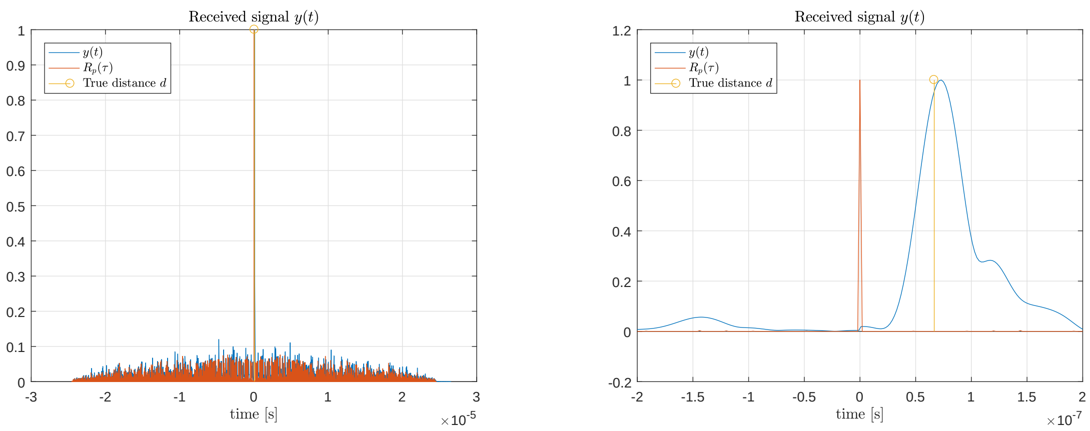

(a) *$y(t)$ and $R_p(\tau)$ plotted.* **(b)** *Zoomed on maximum correlation area.*

Figure 4.9: *Search method for first path delay.*

The method for finding the delay which represents the direct path is by using several shifted cross correlators at the receiver. The cross correlator obtaining the highest correlation level will be chosen as the first arriving peak.

This can be seen as a sweep of $R_P(\tau)$ over the received signal $y(t)$ to find the maximum correlation. The timeshift yielding the maximum correlation is chosen as the delay τ_0 (first path signal). For further description of this cross correlation receiver (RAKE receiver), see [19].

Calculating the maximum of the average of a series of autocorrelation function, it is possible to determine the maximum of these as seen on fig. 4.9b. The series of different autocorrelations utilised for averaging is found on fig. 4.10a, together with the average marked as the black line and the true distance marked with a red stem. The error found by using this method in different SNR-levels is seen on fig. 4.10b.

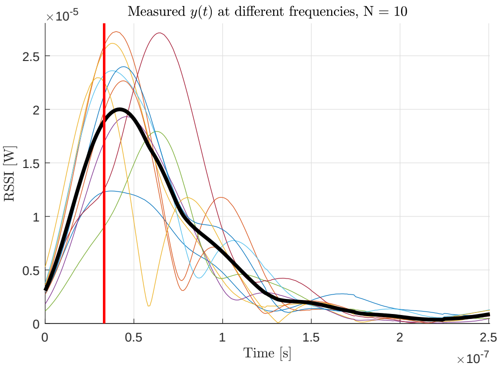

(a) *A series of measured correlation functions. It is seen that depending on the measurement the maximum peak of the cross correlation changes. The average correlation is the black line, and the true distance is the red vertical line.*

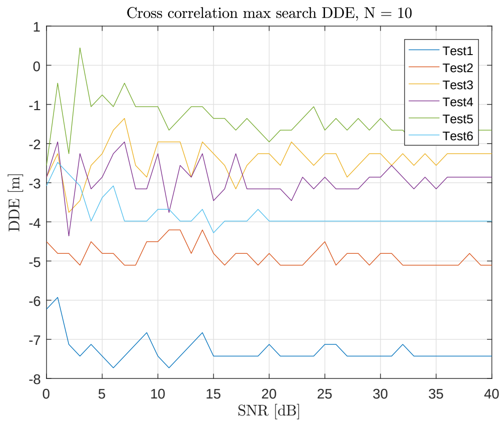

(b) *The average error found in different SNR levels for test 1-6 from appendix A.* $N = 10$, $B = 40MHz$.

Figure 4.10: *Search method for first path delay.*

It is seen that the cross correlation estimates distances so that the DDE error lies between 0 and 7.5 m, this is for measurements performed at 0-20 m, however it is expected that for longer transmission ranges the DDE will increase.

Two approaches can be used to utilise this correlation and peak detection more efficient. Either the bandwidth B of the system has to be increased to obtain higher time resolution or the correlation measured can be utilised as input for the MUSIC algorithm.

4.7 MUSIC Algorithm

As it has been shown, the usage of cross correlation for estimating time of arrival is not suitable for an indoor environment due to the severe multipath scattering which potentially changes the point of maximum correlation, thereby introducing an estimation error. The maximum cross correlation detector has its performance improved by increasing the bandwidth of the transmitted sequence $p(t)$, however for practical purposes this has been shown difficult. Therefore by deploying an advanced signal processing algorithm, namely the MUSIC algorithm, low bandwidth ToA systems can be improved by applying prior knowledge of the system, e.g. knowing the PRN sequence.

Recall the multipath model from eq. (4.17):

$$h(t) = \sum_{i=0}^{K-1} \alpha_i \cdot e^{j\phi_i} \delta(t - \tau_i) \tag{4.25}$$

where $K-1$ is the amount of multipath scatters, α_i is the attenuation, ϕ_i is the phase and τ_i is the propagation delay.

To use the music algorithm a model has to be established fist. A linear combination of autocorrelation functions can be utilised to describe the received signal $\bar{y}$.

The following model and vector notation from [20] will be used:

$$\bar{y} = \bar{A} \cdot \bar{u} + \bar{w} \tag{4.26}$$

where

$$\bar{y} = \begin{bmatrix} y(0) & y(1) & \cdots & y(K-1) \end{bmatrix}^T \tag{4.27}$$
$$\bar{A} = \begin{bmatrix} R_P(\tau_0) & R_P(\tau_1) & \cdots & R_P(\tau_{K-1}) \end{bmatrix}^T \tag{4.28}$$
$$\bar{u} = \begin{bmatrix} u_0 & u_1 & \cdots & u_{K-1} \end{bmatrix} \tag{4.29}$$
$$\bar{w} = \begin{bmatrix} w(0) & w(1) & \cdots & w(K-1) \end{bmatrix}^T \tag{4.30}$$
$$\tag{4.31}$$

where u is the complex weights $\alpha_i \cdot e^{j\phi_i}$ from the channel eq. (4.25) and $R_P(\tau)$ is the autocorrelation of the PRN sequence shifted by τ. $\bar{w}$ is additive white noise.

The MUSIC algorithm is as mentioned earlier based on the eigenvalue decomposition of the covariance matrix of the autocorrelation functions described by eq. (4.26). From [19] the input covariance matrix for the MUSIC algorithm is described as eq. (4.32):

$$\bar{C} = E[\bar{y}\bar{y}^*] \tag{4.32}$$

which by inserting eq. (4.26) results in eqs. (4.33) and (4.34).

$$\bar{C} = \bar{A}E[\bar{u}\bar{u}^*]\bar{A}^* + E[\bar{w}\bar{w}^*] \tag{4.33}$$
$$\bar{C} = \bar{A}C_{uu}\bar{A}^* + C_{ww} \tag{4.34}$$

Assuming the noise $\bar{W}$ to be AWGN, eq. (4.34) can be written as:

$$\bar{C} = \bar{A}C_{uu}\bar{A}^* + \sigma_w^2\bar{I} \tag{4.35}$$

where σ_w is the standard deviation of the noise and $\bar{I}$ is the identity matrix. The subspaces used in the MUSIC algorithm may now be found by eigenvalue decomposition to obtain $\bar{A}$ and C_{uu}.

For now lets assume that the magnitude α_i is constant and the phase ϕ_i is random uniformly distributed $\in [0, 2\pi]$ over the different propagation delays τ_i. In this case it is known that the rank of the covariance matrix is full for a $K \times K$ matrix, and also the $K \times K$ matrix is non-singular.

Having $J > K$ measurements, from linear algebra and the theory of noise estimation it is known that the $J \times J$ covariance matrix formed by J measurements will have rank K. Therefore it is also seen that the $J-K$ smallest eigenvalues are all equal to the noise σ_W^2. It should be noted that the K largest eigenvalues are associated with K signal eigenvectors, and that the $J - K$ smallest eigenvectors are associated with noise eigenvectors.

The remarkable property of the noise and signal eigenvectors is the fact that the subspace spaced by the noise eigenvectors are orthogonal on the subspace spaced by the signal eigenvectors.

Denoting the eigenvectors by β_i there exists β_i for $i = 0 \ldots K$ signal eigenvectors and β_i for $i = K + 1 \ldots J$ noise eigenvectors with the orthogonal property. From the orthogonal property the autocorrelation $R_P(\tau)$ can be used as a projection of the signal subspace onto the noise subspace, see eq. (4.36).

$$\bar{\beta_i}^* \cdot \bar{R_p}(\tau) = 0 \tag{4.36}$$

As $R_p(\tau)$ must lie within the signal subspace, using the orthogonal subspace to create a pseudo spectrum, the time delay τ_0 complying with the orthogonality will be shown as a spike in the MUSIC spectrum given by eq. (4.37):

$$M(t) = \frac{1}{\displaystyle\sum_{i=K+1}^{J} \beta_i^* \cdot R_P(\tau_i)} \tag{4.37}$$

For more information on the MUSIC algorithm and its properties, see [12–15, 19, 20].

The Music algorithm requires the covariance matrix for the signal as input. For simulations this is easily obtained as the noise and signal vectors are generated separately as in eq. (4.35). However for the measured signals the covariance matrix has to be estimated using the observations, the estimated covariance matrix is denoted $\hat{C}$ defined in eq. (4.38):

$$\bar{\hat{C}} = 1/L \sum_{i=1}^{L} \bar{y}\bar{y}^* \tag{4.38}$$

where L is amount of snapshots of the received signal.

A block diagram showing the different steps in the MUSIC algorithm is found on fig. 4.11.

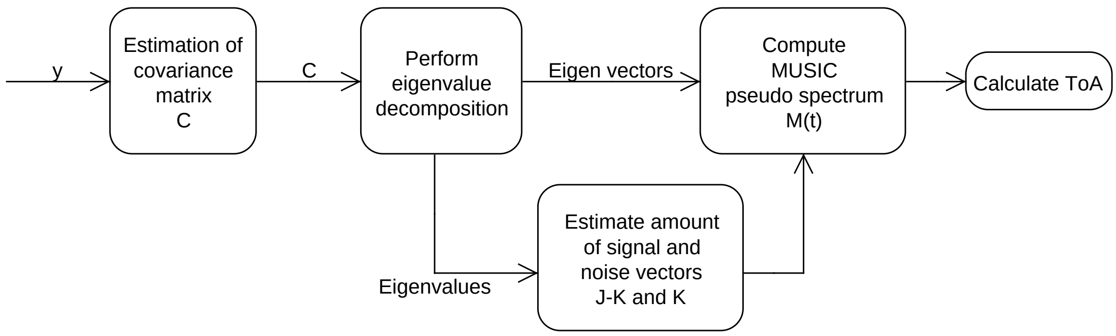

Figure 4.11: *Block diagram showing different steps in the MUSIC algorithm.*

4.7.1 Decorrelating the Covariance Matrix

It was assumed that the phase ϕ of the received signals were uniformly distribute between $[0, \pi]$ and the attenuation α was constant for the signal propagation delay τ. However for a practical scenario often described by the wide sense stationary uncorrelated scattering (WSSUS) channel, the complex attenuation $u = \alpha e^{j\phi}$ is highly correlated, and to avoid ambiguities uncorrelated data has to be used for input to the MUSIC algorithm. To obtain uncorrelated data the wireless channel is measured over a set of different frequencies. The amount of frequencies used is given by N. For each different frequency the covariance matrix C is calculated. Denoting each different covariance matrices by C_i the uncorrelated covariance matrix is given by eq. (4.39):

$$\bar{\hat{C}} = \frac{1}{N}\sum_{i=1}^{N}\bar{C}_i \tag{4.39}$$

Other methods can also be used to calculate a more precise covariance matrix, these are briefly mentioned. Other techniques could be the use of spatial smoothing using several measurements in different manners to obtain a more precise covariance matrix. Another method is the usage of a Forward-Backward algorithm used to calculate a better estimate of the covariance matrix by making it more like a Teoplitz matrix (equal elements along the diagonal of the covariance matrix). The Forward backward algorithm is implemented using

$$\bar{\hat{C}}^{FB} = \frac{1}{2}(\bar{\hat{C}} + J\bar{\hat{C}}^{*}J) \tag{4.40}$$

where J is the anti diagonal matrix of size $K \times K$.

The methods for more precise covariance matrices are not used further.

Chapter 5

MUSIC Algorithm Performance Analysis

The system model has been simulated and evaluated w.r.t different parameters when changes the performance of the system. The following chapter describes and concludes the results. The following sections will describe how the evaluations were made both for simulated and empirical data. The largest difference between the simulations and the measurements is the level of correlation together with the amount of reflections, where for simulated data few reflection are used and the measurements captures all the reflections for the given scenario.

For the simulations uncorrelated channels have been simulated, however for the measured channels the different scatters might not be fully uncorrelated, and as the MUSIC algorithm requires full rank and uncorrelated data the performance might decrease, to obtain uncorrelated data see section 4.7.1. In simulations the scatters have same power, however for the measured wireless channel it is seen that the reflections are often attenuated compared with the direct path peak.

The parameters tested is the SNR, the bandwidth B, the different path delays τ, the peak-estimation and the amount of samples in both time and frequency, snapshots in time will be denoted L and frequency will be denoted N. Both different NLOS and LOS situations are measured and evaluated.

Analysing the performance of the MUSIC algorithm is dependent on several input parameters, and a full evaluation of these will not be made in this project.

When referring to a "test" these are the different measurements from appendix A.

5.1 Analytical 2-path tests

The following section will describe the evaluation of the performance using the MUSIC algorithm with a simulated wireless channel. The simulations provides insight in the performance in a controlled environment, where different aspects of e.g. the wireless channel can be controlled. Performance of a ToA system is measured by its ability to detect the first arriving peak of a signal, τ_0.

Therefore an evaluation of the detection performance for two peaks were made. The peaks were set were with a static $\Delta t = \tau_1 - \tau_0$, where τ_0 is the ToA of the first arriving peak and τ_1 is the arrival of a delayed peak.

The simulated channels have been normalized w.r.t. the bandwidth of the system, B.

The simulation was tested on a channel as seen on fig. 5.1 where for different tests, variations in Δt are introduced. The MUSIC spectrum, M(t), calculated for the channel can be found on fig. 5.2. It is clearly seen that $M(t)$ indicates that two paths are found in the channel and the marked delays, τ, corresponds well with the simulated delays from fig. 5.1. The simulations were made using SNR = 25 dB, number of time snapshots $L = 10$ and number of frequencies $N = 10$.

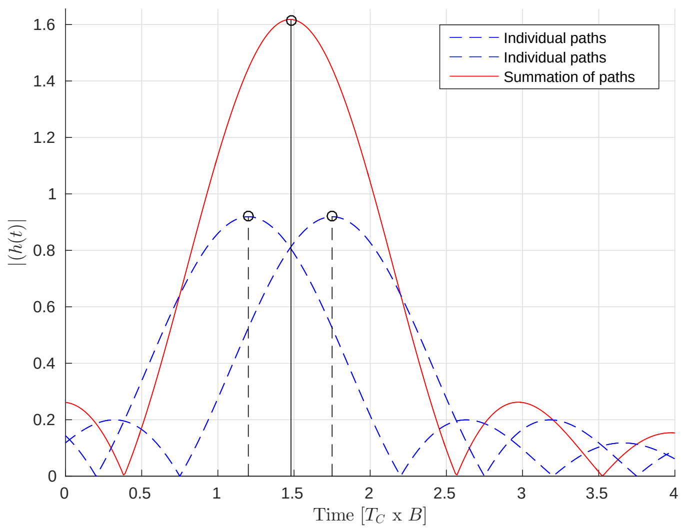

Figure 5.1: *The simulated channel, with two delays $\tau_0 = 1.2$ and $\tau_1 = 1.75$. $\Delta t = 0.55$.*

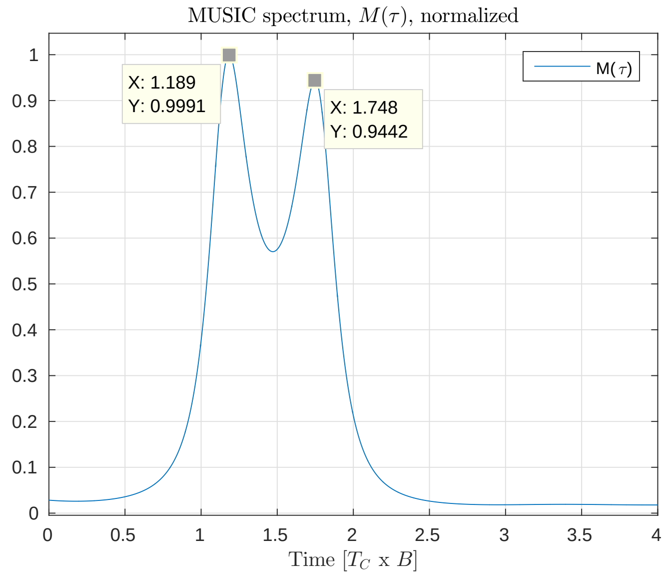

Figure 5.2: *MUSIC spectrum calculated for simulations with channel from fig. 5.1. It is easily seen that the peaks at $\tau_0 = 1.2$ and $\tau_1 = 1.75$ are found. SNR = 25 dB, L = 10, N = 10.*

The evaluation of the required SNR with regards to detecting τ_0 and how this is impacted by the different SNR and Δt is found on fig. 5.3. For these simulations N = 10 different frequencies has been used to obtain uncorrelated data, and $L = 20$ different time-snapshots has been taken for each frequency resulting in a total of 200 snapshots.

The error in detectability is the DDE given by eq. (2.9). It is the mean error from the true distance ,d, to estimated distance ,$\hat{d}$. Calculating an actual distance would require that the bandwidth, B, is known.

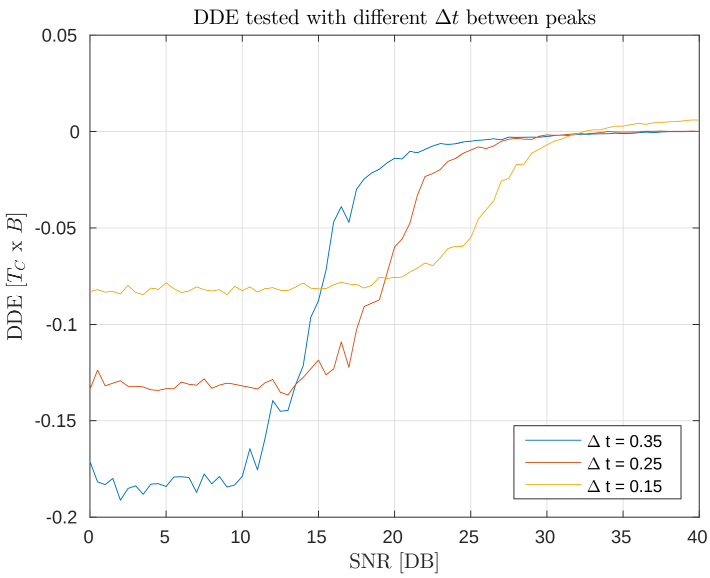

Figure 5.3: *Test of the ability to detect τ_0 with changing Δt and at different SNR. $L = 20$ and $N = 10$.*

For the purpose of detecting the time of arrival τ_0 it can be seen on fig. 5.3 that the DDE is better when the two peaks arrives within a short Δt of each other. The curve from $\Delta t = 0.15$, achieves the best DDE at SNR from 0-15 dB compared with other Δt-tests. At the low SNR compared with the other tests, having peaks arrive close to each other still seems to obtain satisfying accuracy. This is explained by the fact that two paths arriving within a short Δt will be seen as a single path by the system. Therefore the DDE in the case that the two paths has equal power becomes half the time difference, $DDE = \frac{\Delta t}{2}$.

For two close arriving paths, the DDE is good for low SNR (0-15 dB), however a higher SNR than that required to obtain low DDE for the case of $\Delta t = 0.25$ and $\Delta t = 0.35$ is required to obtain the exact distance. This is because the paths arrives close to each other ($\delta t = 0.15$) and therefore higher SNR is required to distinguish these. This is only the case when the paths have equal power and only two paths are present.

The impact of the amount of uncorrelated samples have been tested. The method for obtaining uncorrelated samples in the WSSUS channel is to make frequency hopping over N different frequencies. The simulations are made at 50 iterations for each SNR, and afterwards an average is calculated. It can be seen that changing from $N = 10$ to $N = 25$, the SNR required to obtain the same DDE is lowered by approximately 4-5 dB, see fig. 5.4.

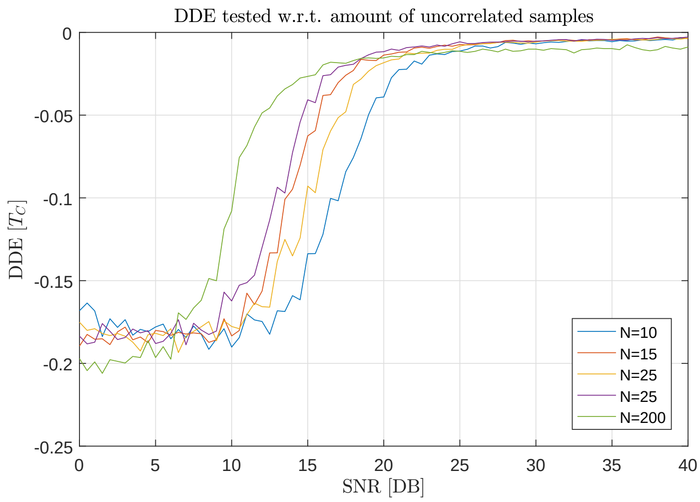

Figure 5.4: *Changes in amount of different frequencies N, to examine impact of DDE at different SNR levels.* $L = 10$.

The DDE improvement using $N = 200$ has also been simulated. From this it can be seen that having enough uncorrelated data, even for SNR levels from 0-15 dB it is possible to obtain a low DDE. However in a practical scenario it might not be possible to obtain this amount of uncorrelated frequencies as there are limitations in the frequency band available, for further information of obtainable uncorrelated frequencies see appendix A.5. The evaluation of measured wireless channels correlation impact is found in section 5.3.

5.2 Experimental evaluation of MUSIC algorithm

In order to analyse the performance in a real life implementation, 6 different scenarios has been measured, 3 LOS and 3 NLOS setups. The 3 LOS measurements are the same scenario but with an increasing distance between transmitter and receiver. For a description of how the different setups were measures see appendix A. The different measured wireless channels and their corresponding frequency sweeps are found in appendix A.4.

A measured LOS and NLOS channel from appendix A are found on fig. 5.5. Note that the NLOS has a large attenuation of its first peak arrival in the NLOS case, see fig. 5.5b. The figures are created w.r.t. distance on the x-axis.

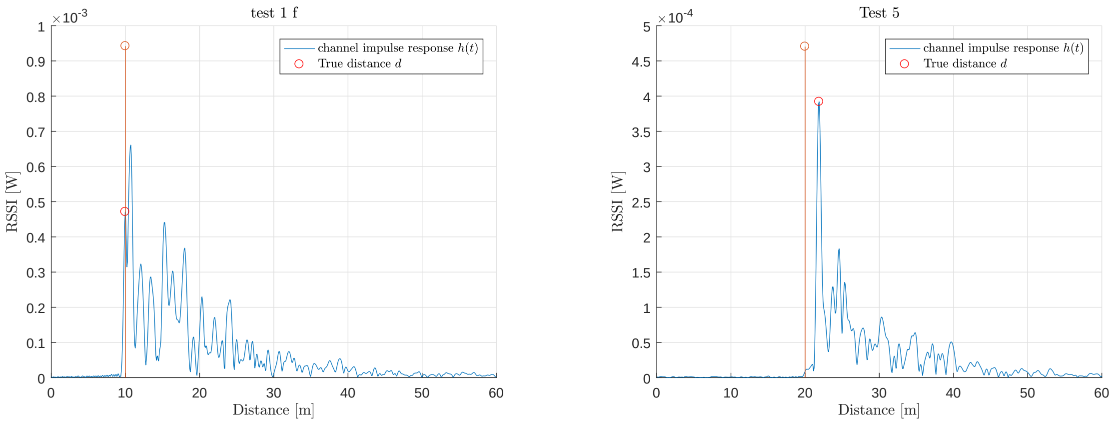

(a) *Test 1, LOS condition,* $B = 1GHz$.

(b) *Test 5, NLOS condition,* $B = 1GHz$.

Figure 5.5: *Channel impulse response* $h(t)$ *for two different measurements of wireless channel.*

The measurements result in a set of impulse responses. To obtain the covariance matrix used for MUSIC algorithm input, simulations has been made transmitting a PRN Gold Code sequence through the measured wireless channel and correlating the received signal with a replica of the transmitted sequence, see sections 4.5 and 4.6. The correlations now obtained is utilised to calculate the covariance matrix using eq. (4.38) and eq. (4.39) used as input for the MUSIC algorithm, see section 4.7. fig. 5.6 is showing 10 different measured correlation functions, from N = 10 different frequencies.

The SNR is tested by adding white noise to each impulse response. The SNR is measured by calculating the variance of the measured channel signal and scaling the added noise correspondingly to obtain the given SNR.

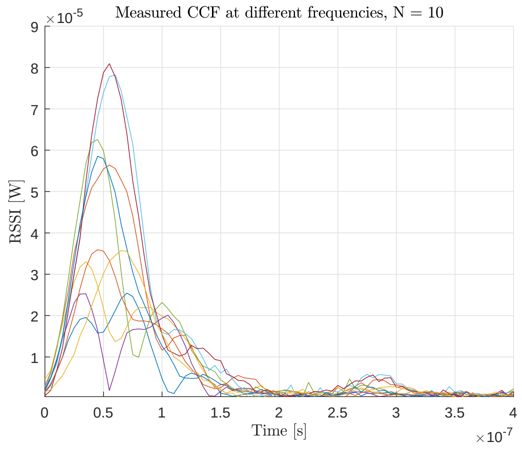

Figure 5.6: *Measured CCF from 10 different frequencies. Gold code is assumed for the transmitting PRN sequence. Figure is only showing the relevant sample area.* $B = 40MHz$.

Using the covariance matrix as input for the MUSIC algorithm, the corresponding MUSIC Spectrum $M(t)$ obtained can be seen on fig. 5.7d. The first peak of the music spectrum is detected at 42 ns and it is known that the true peak is 38.3 nS(11.5 m) therefore this measured peak of the spectrum results in a DDE of only 1.11 m.

The procedure mentioned above has been utilised with the 6 different scenarios mentioned, for more information see appendix A, to evaluate the performance of the DDE for each scenario. The DDE has been tested at different SNR levels. Tests have been made at $B = [40, 60, 80]$ MHz and with 20 iterations for each tested SNR for each scenario at each bandwidth.

The evaluations of the bandwidth B is found on figs. 5.7a to 5.7c and how this impacts the music spectrum for one of the test is found on fig. 5.7d.

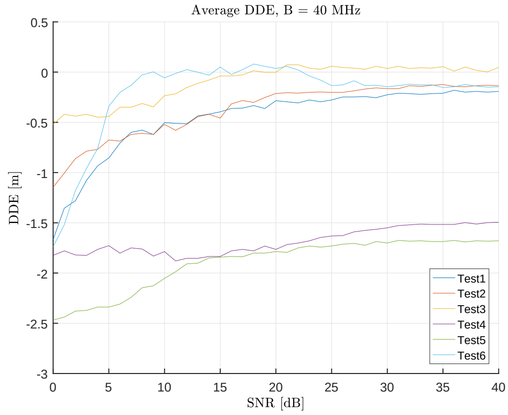

(a) *B = 40 MHz, measured DDE for test 1-6.*

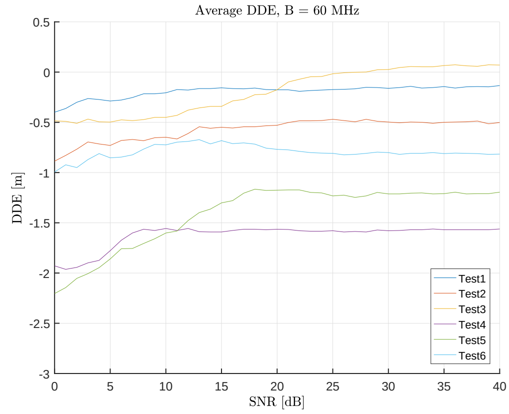

(b) *B = 60 MHz, measured DDE for test 1-6.*

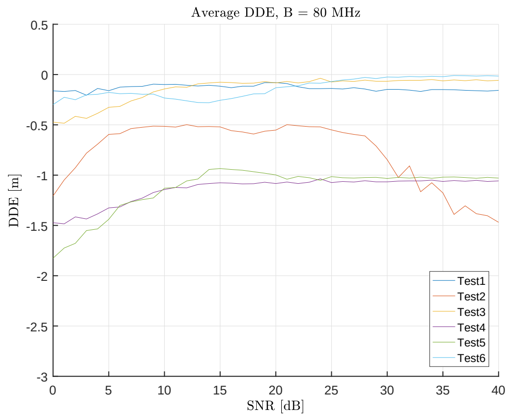

(c) *B = 80 MHz, measured DDE for test 1-6.*

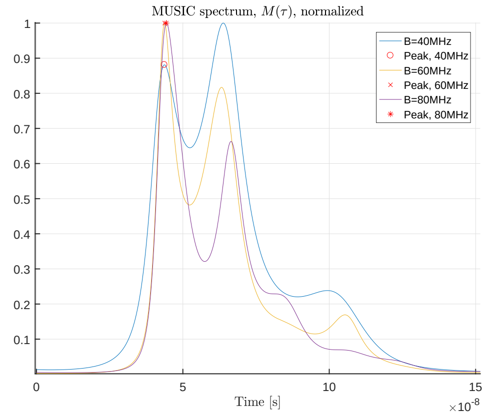

(d) *Measured music spectrum at B = [40,60,80] MHz. Measurement used is test 6.*

Figure 5.7: *Evaluation of different input parameters for MUSIC algorithm. L = 20 and N = 10 for all tests.*

It is seen that the accuracy increases with an increasing bandwidth. Also as test 1-3 are the LOS and test 4-6 are NLOS it is also noted that for the NLOS situations the DDE is the worst at 1.5-2.5 m accuracy at SNR = 0 dB. For the LOS situations a DDE generally below 1 m can be achieved except for the 40 MHz bandwidth where the accuracy of 1 m for LOS is first achieved for SRN > 10 dB.

The most important from the DDE results is that by using the MUSIC algorithm the accuracy achieved is better than that achieved by the use of correlation max search from fig. 4.10b. The correlation maximum search achieves accuracies for test 1-6 in between 1 - 7 m with a bandwidth $B = 40$ MHz. The MUSIC algorithm with same system parameter enhances the time resolution thereby achieving accuracies between 0 - 2.5 m. Where looking solely on the LOS cases the accuracies lies between 0-1.5 m.

Similar performance for the MUSIC algorithm and correlation max search can be found in [19], where for a larger set of empirical data the following MUSIC and correlation search CDF is found, see fig. 5.8.

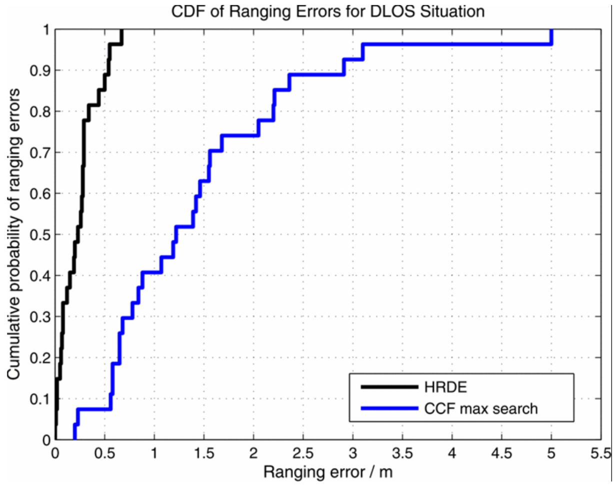

Figure 5.8: *Resulting correlation search (CCF max search) and Music Algorithm(HRDE) for empirical measurements performed in [19].*

5.3 Correlation impact

As the MUSIC algorithm requires a full rank covariance matrix as mentioned in section 4.7, the performance depending on the amount of frequencies used to obtain uncorrelated data has been evaluated. Using $B = [40, 60, 80]MHz$ and N = [10,15,20] different frequencies the DDE of test 1 has been calculated to give an indication of the impact of frequency amount and bandwidth changes. The result is shown on fig. 5.9.

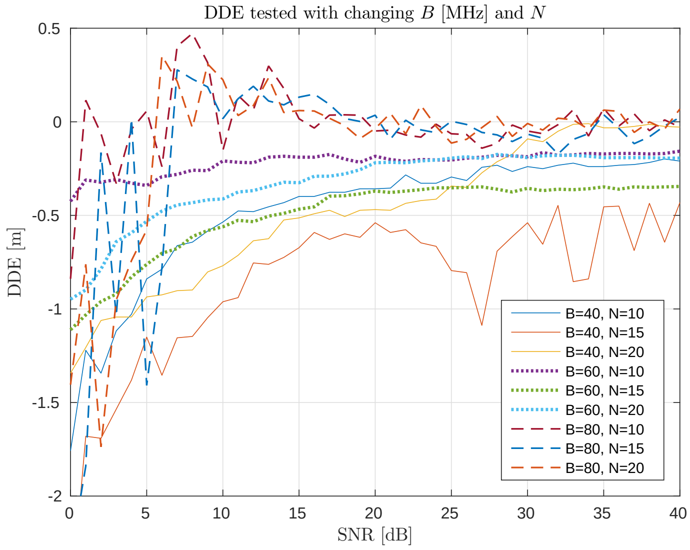

Figure 5.9: *The decrease of DDE at different SNR levels depending on B and N.*

It is seen that the amount of uncorrelated data does not seem to have a definitive impact, It can be seen that increasing the amount of uncorrelated data N both has possibility to increase or decrease the DDE. It can however be seen that increasing the bandwidth of the system B increases the accuracy. Especially the line of sight measurements accuracy are increased whereas the DDE for the NLOS measurements saturates towards the first detectable peak of impulse responses. This is also backed by [13, 19] stating that it is more important to have high time resolution on the measured auto correlation functions used as input for the MUSIC algorithm, than having a lot of frequency snapshots N.

The difficulty might be to create a system with a wide bandwidth, compared to creating a narrowband system. Therefore the pros and cons for creating a real life implementation should be a weighting between complexity of the system and acceptable accuracy and precision.

5.4 Measurement precision and accuracy

The precision of the measurements are dependent on the SNR. At lower SNR the fluctuations of the DDE is higher than at larger SNR. As small DDE can be achieved using different uncorrelated frequencies and a high bandwidth, it does not mean that large errors can not occur. Also even though the DDE saturates the precision of the measurements still allow for large errors. Test 3 has been used as a LOS case where the error distribution for different SNR levels has been evaluated. The distributions of error was found to be normal distributed with mean μ and standard deviation σ, from the error data a fitting of a normal distribution was made. The PDF of this is found on fig. 5.10 for SNR levels of $[0, 10, 20]$.

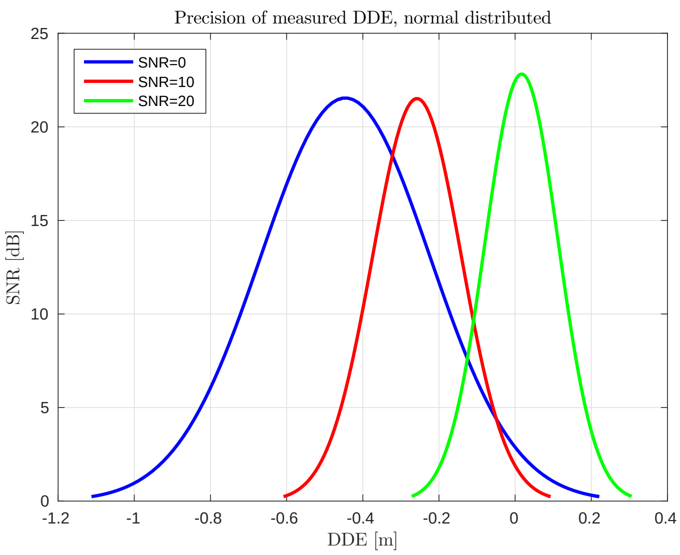

Figure 5.10: *Fitted PDF of DDE at different SNR-levels. B = 40 MHz, L = 20, N = 10. Test 3 was used to generate PDF.*

In table 5.1 is found a mean(accuracy), μ, and standard deviation, σ,(measure of precision) averaged over test 1-6. At low SNR both the accuracy and the precision are low, even with a lot of measurements the accuracy will not reach a mean of 0 m, but saturates towards it. However as the SNR increases it is seen, as expected, that the standard deviation, σ, decreases.

SNR [dB]	0	1	2	3	4	5	10	20	30	40
μ [m]	-1.04	-0.97	-0.88	-0.81	-0.75	-0.66	-0.5	-0.25	-0.23	-0.22
σ	0.4	0.33	0.29	0.22	0.22	0.2	0.117	0.08	0.067	0.046

Table 5.1: *Mean and standard deviation of measurements at different SNR levels. Saturation in both accuracy and precision is observed.* $B = 40$ *MHz.*

5.5 Signal Space Evaluation

It is important to note that due to the method of eigenvalue decomposition used in the MUSIC algorithm, it is a critical point of interest to investigate the changes in accuracy by choosing a wrong amount of noise eigenvectors to use for music spectrum estimation, see section 4.7. As the covariance matrix will hold K signal vectors and $J - K - 1$ noise eigenvectors, where J is the rank of the covariance matrix, it is important to choose the correct amount of noise eigenvectors. The amount of noise vectors to use $J - K - 1$ will be refered as V. Using test 1 the impact of choosing V incorrect evaluated. For more information on the amount of vectors, see the eigenvalue decomposition mentioned in section 4.7.

A stem plot of the eigenvalues is found on fig. 5.11a, it can be seen that there exists 3 eigenvalues larger than σ_w^2. Thoose the amount of noise eigenvectors to use for estimation of the spectrum is $V = J - K - 1 = 77$ as the rank of the covariance matrix is 81. Testing the amount of eigenvectors to estimate the spectrum from $V = 1 \ldots 81$ can be seen on fig. 5.12. It is expected to see a saturation after $V > 3$ as no signal vectors are used for MUSIC spectrum estimation.

It can be seen on fig. 5.11b that at lower SNR it can be difficult to estimate k therefore introducing large errors. To overcome this problem choosing $V << J - K - 1$ than an initial estimate of the amount of signal vectors is preferred as seen on fig. 5.12 which shows saturation even for choosing the amount of noise eigenvectors lower than the initial guess.

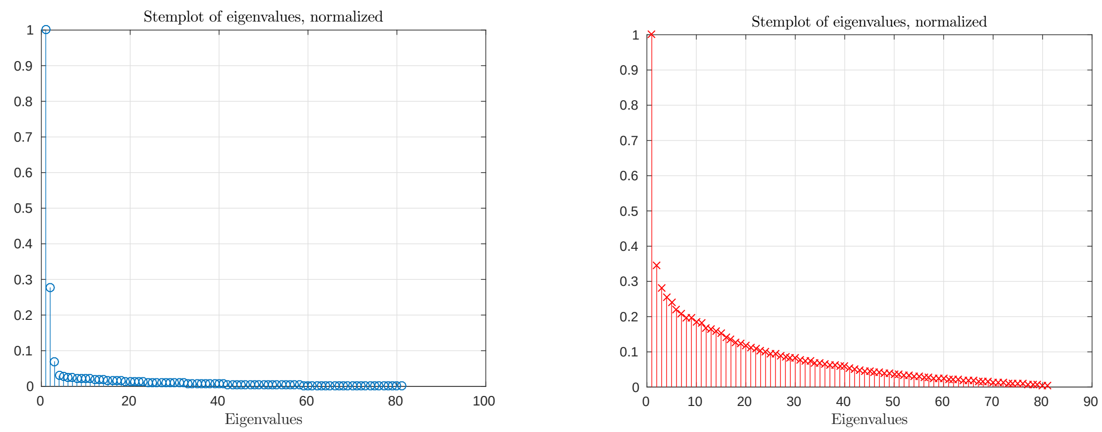

(a) *B = 40 MHz. SNR = 20 dB.* **(b)** *B = 40 MHz. SNR = 0 dB.*

Figure 5.11: *Stemplot of eigenvalues for the EVD of the covariance matrix. L = 20, N = 10.*

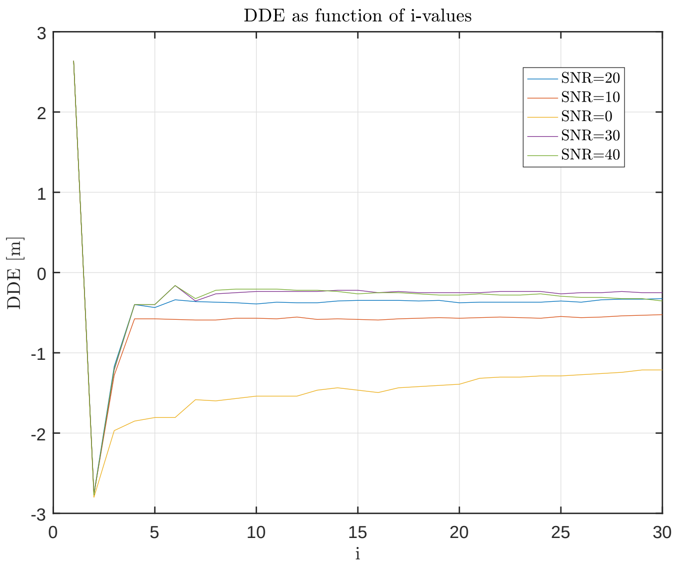

Figure 5.12: *Choice of i values for estimation for the MUSIC spectrum, $M(\tau)$. J tested from 1-30 as saturation is already introduced in the earlier J-values.*

Chapter 6

Conclusion

In this thesis the basic performance of indoor localisation systems was investigated. Chapter 3 consist of an analysis of different methods for indoor positioning, both the methods used to calculate the positions of a tag, and the wireless channel characteristics which can be used to calculate input data for the positioning methods. Signal strength, Time of Arrival and Angle of Arrival was investigated to evaluate the performance especially w.r.t. the changes in a wireless channel and the errors this introduces. The Time of Arrival system was concluded the most promising technique and the thesis transitioned into an analysis of this.

For ToA as measure of distance different ToA detection methods was investigated. These being the general approach of using a correlation maximum search based on correlation properties of the pseudo random noise codes used. And the use of the MUSIC algorithm to estimate the ToA based on a eigenvalue decomposition of the signal thereby exploiting the properties of the signals to increase time resolution for better accuracy.

Further in chapter 4 a system description and model for a ToA system is described used for further simulation of the system and for describing what factors should be taken into consideration in a real life implementation. The evaluation of the correlation search is also made and it is shown that accuracies for both LOS and NLOS in the area of 1 - 7 m can be achieved using both simulated and empirical data. Lastly the section presents the MUSIC algorithm and describes the steps to obtain the MUSIC spectrum $M(t)$.

Chapter 5 evaluates the MUSIC algorithm for simulations of the model described for a ToA system. For simulations the impact of scatter arrival, SNR and correlation was evaluated. The measurements performed are examined and the MUSIC spectrum is used to estimate the ToA of the first peak for the measured channels. Depending on the SNR, accuracies < 2.5m can be obtained for NLOS situations and errors < 1m can be achieved for LOS situations. It is also found that increasing the bandwidth B of the system increases performance of the accuracy. Going from $B = 40MHz$ to $B = 80MHz$ improves the accuracy by 0.5-1 m. For SNR levels tested it is seen that the precision increases with increasing SNR, however for the empirical data the accuracy with enough measurement does not seem to change. The amount of uncorrelated data was investigated and it is found that 10 sets of uncorrelated frequencies are sufficient for achieving good accuracy. It is seen from the NLOS cases that the estimation error has limitations for this case as an undetected direct peak will not be present in the MUSIC spectrum.

The MUSIC algorithm is capable of enhancing the traditional method of correlation max search. The higher time resolution provided for low bandwidth systems gives a significant improvement in accuracy however it also increases the complexity of a system. ToA with higher precision is possible to create using the MUSIC algorithm.

6.1 Future Work

As the MUSIC algorithm has been used and is a known signal processing technique, several varieties and improvement os this has been developed. For further improving the system and the corresponding DDE results implementations of these even more advance MUSIC algorithms could be made. The MUSIC algorithms which is expected to improve the systems performance is the EV (eigenvector) method. The reason for improvements in this algorithm is that the noise eigenvectors are expecte to all be equal to σ_w^2 for a theoretical implementation. However for an actual estimate covariance matrix the noise eigenvectors are $\neq \sigma_w^2$ and by utilising a normalisation with the eigenvalues it is found in [14] that the MUSIC spectrum is less sensitive to inaccurate estimates of the noise eigenvalues.

Therefore the music spectrum would be given by:

$$M(t) = \frac{1}{\sum\limits_{i=K+1}^{J} \frac{1}{\lambda_i} \beta_i^* \cdot R_P(\tau_i)} \tag{6.1}$$

where λ is the eigenvalue of the corresponding noise vector β_i.

Also implementation of the Forward Backward algorithm mentioned in section 4.7 to obtain a toeplitz matrix could be implemented to further improve the estimation. Another MUSIC variant which is often used or referred to is the ROOT-MUSIC algorithm, this algorithm has however not been further investigated.

Other methods such as the ESPRIT algorithm is also widely used within the estimates of AoA and ToA and should also be implemented and tested.

To evaluate the MUSIC algorithms performance, a more strategic approach to the measurement campaign should be made. This is a result of too few measurement having been made to evaluate the performance of the algorithm. Only 2 actual NLOS situations is seen from the measurements those being test 4 and 5 from appendix A. Especially longer distances between transmitter and receiver should be measured and the performance in these situations should be evaluated against the performance of a corresponding correlation max search. It is also important to measure the wireless channels over time to see the fluctuations and estimate the SNR level whereas a more precise estimate of the impact of noise could be performed.

Further investigation woule also include a prototype for ToA measuring or several prototypes for setting up a TDoA system for testing and in- or decreasing accuracy using this system with the MUSIC algorithm.

For Further work should also be described the impact of the modulator and demodulator, together with a description of the errors these could introduce.

Bibliography

[1] "Indoor location market by component," 2016.

[2] R. N. Zahid Farid and M. Ismail, "Recent advances in wireless indoor localization techniques and system," *Journal of Computer Networks and Communications*, vol. 2013, pp. 1–12, 2013.

[3] H. Liu, H. Darabi, P. Banerjee, and J. Liu, "Survey of wireless indoor positioning techniques and systems," *IEEE Transactions on Systems, Man, and Cybernetics, Part C (Applications and Reviews)*, vol. 37, pp. 1067–1080, Nov 2007.

[4] HP Invent, *SmartLOCUS: An autonomous, self-assembling sensor network for indoor asset and systems management*, June 2005.

[5] M. Werner, *Indoor Location-Based Services*. Springer, 2014. ISBN:978-3-319-10698-4.

[6] T. L. Beomju Shin, Jung Ho Lee and H. S. Kim, "Enhanced weighted k-nearest neighbor algorithm for indoor wi-fi positioning systems," *Computing Technology and Information Management (ICCM)*, pp. 574–577, 2012.

[7] A. Ibrahim, S. K. A. Rahim, and H. Mohamad, "Performance evaluation of rss-based wsn indoor localization scheme using artificial neural network schemes," in *2015 IEEE 12th Malaysia International Conference on Communications (MICC)*, pp. 300–305, Nov 2015.

[8] L. S. Gus German, Quentin Spencer and R. Valenzuela, "Wireless indoor channel modeling: Statistical agreement of ray tracing simulations and channel sounding measurements," *Acoustics, Speech, and Signal Processing, 1988*, vol. 18, no. 4, pp. 2501–2504, 2001.

[9] M. A. J. Quentin H Spencer, Brian D Jeffs and A. L. Swindlehurst., "Modeling the statistical time and angle of arrival characteristics of an indoor multipath channel," *IEEE JOURNAL ON SELECTED AREAS IN COMMUNICATIONS*, vol. 18, no. 3, pp. 347–360, 2000.

[10] F. L. Y. Z. Jiuqiang Xu, Wei Liu and C. Wang, "Distance measurement model based on rssi in wsn," *Wireless Sensor Network*, vol. 2, no. 18, pp. 606–611, 2010.

[11] Kegen Yu and Ian Sharp and Y. Jay Guo, *Ground-Based Wireless Positioning*. John Wiley & sons Ltd.

[12] L. Jing, P. Liang, C. Maoyong, and S. Nongliang, "Super-resolution time of arrival estimation for indoor geolocation based on ieee 802.11 a/g," in *2008 7th World Congress on Intelligent Control and Automation*, pp. 6612–6615, June 2008.

[13] R. K. Michael Marx and H. C. Müller, "High resolution delay locked loop for time synchronization with multi path mitigation," *Research in Microelectronics and Electronics*, pp. 204–207, 2009.

[14] X. Li, *Performance of TOA Estimation Algorithms in Different Indoor Multipath Conditions*. Worcester Polytechnic Institute, 2003. Master Thesis.

[15] H. Farrokhi, "Toa estimation using music super-resolution techniques for an indoor audible chirp ranging system," in *2007 IEEE International Conference on Signal Processing and Communications*, pp. 987–990, Nov 2007.

[16] "Quadrature iq." Seen: 2017-02-22.

[17] "Gold code sequence," 2008. Seen: 2017-02-15.

[18] R. Gold, "Optimal binary sequences for spread spectrum multiplexing (corresp.)," *IEEE Transaction on Information Theory*, vol. 13, no. 4, pp. 619–621, 1967.

[19] M. Marx, "System issues for time synchronization in real time localisation systems with multi path mitigation," *2010 European Wireless Conference*, pp. 596–601, 2010.

[20] N. A. Alsindi, *Super-Resolution TOA Estimation with Diversity Techniques for Indoor Geolocation Application*. Worcester Polytechnic Institute, 2004. Master Thesis.

Appendix A

Channel Measurement Description

A.1 Purpose of Measurements

To evaluate the MUSIC algorithm in a real life implementation it is important to have measurements for a different set of scenarios and distances. Simulations does not represent the wireless characteristics to same degree as actual measurements which captures both attenuations and multipath effects. The following appendix will describe how the different measurements were conducted, and how the post-processing of frequency- and time-domain data were made.

A.2 Setup

For measuring the wireless channel a network analyser, namely the Agilent N5227A version A.09.80.20, was used.

A frequency sweep were measured from $f = 2\,\text{GHz} - 3\,\text{GHz}$ with a frequency stepping of $\Delta f = 500$ KHz.

For transmitting and receiving antenna were used two Suhner SWA 0859/360/4/10/V planar antennas. The antenna pattern at the frequency range does not change much, therefore patterns only for 2.3 GHz and 2.7 GHz is shown, see figs. A.1a and A.1b.

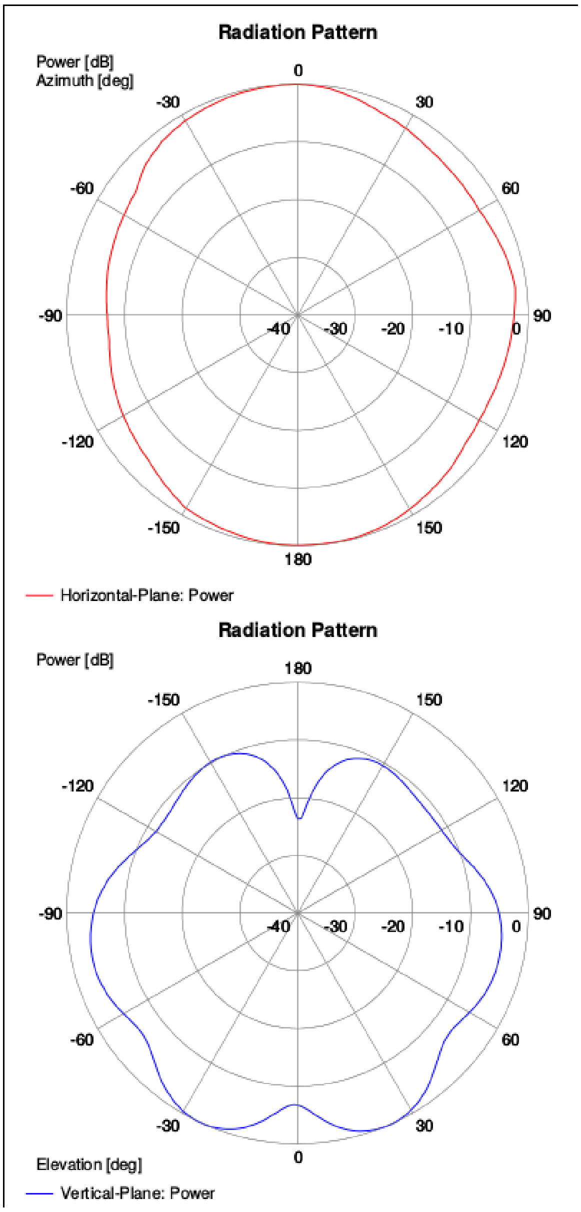

(a) *2.3 GHz behaviour of antenna.*

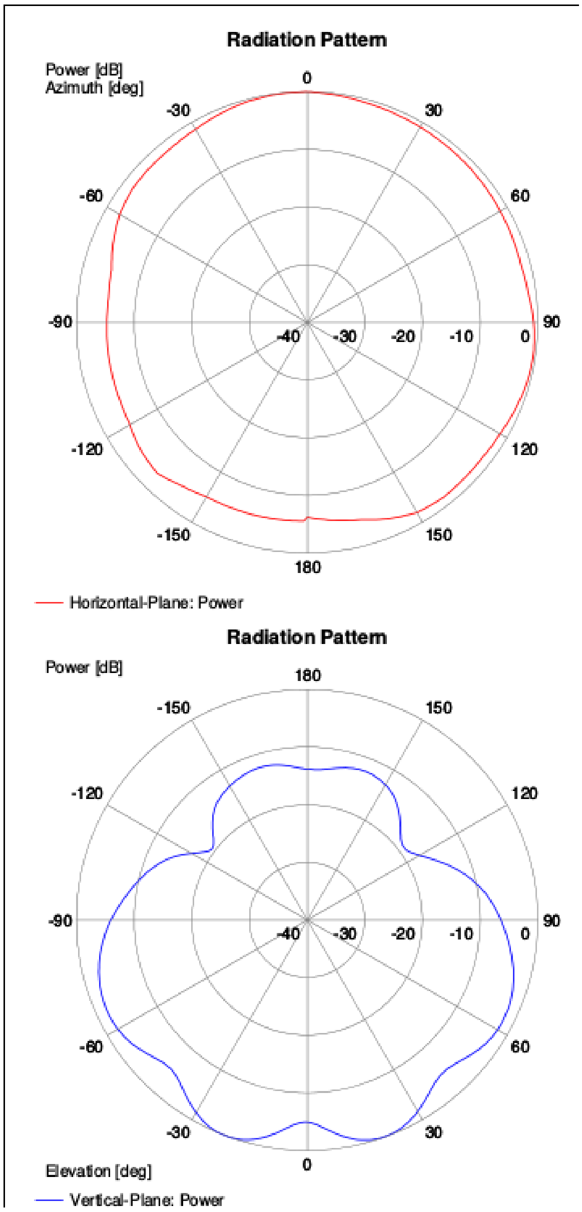

(b) *2.7 GHz behaviour of antenna.*

Figure A.1: *Antenna pattern for the planar antenna used for measuring the wireless channel.*

After setting up the Agilent N5227A the cables connecting the antennas to the network analyser is mounted. The impact of the cables, such as extra delay and attenuation is calibrated so that only the wireless channel impact is measured.

The measurements were conducted in the institute of Aalborg university, at the AP-Net(Antenna, Propagation and Radio Networking APNet) section, located at Niels Jernes vej 12, A6 building.

The floor plan for the area the measurements were creates in and positions of transmitter and receiver at the 6 different tests are shown on fig. A.2.

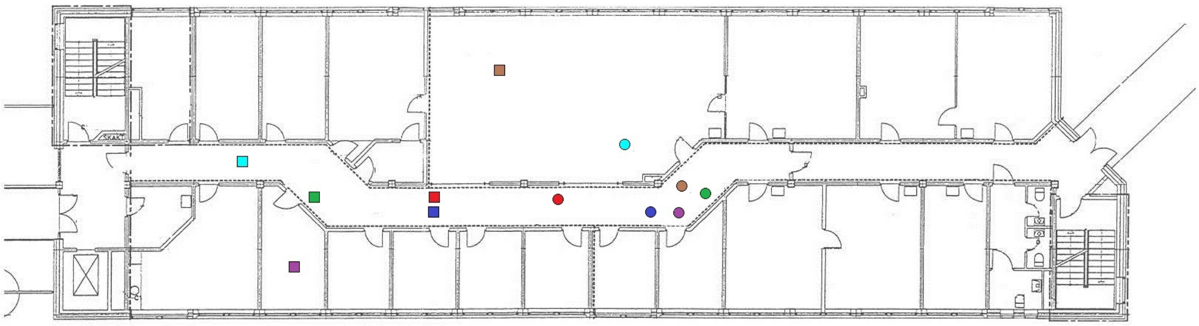

Figure A.2: *Floorplan of measurement area, squares are receiver positions, circles are transmitter positions, colors are matching pairs for each of the 6 tests.*

For summarization of the distance and naming of the different tests and conditions, see table A.1.

Test number	Color	Condition	True distance [m]
1	Red	LOS	10
2	Blue	LOS	15.5
3	Green	LOS	20
4	Cyan	NLOS	20
5	Purple	NLOS	21
6	Brown	NLOS	12

Table A.1: *Listing of the different tests conducted, with color-code to identify on fig. A.2.*

For each setup a single frequency sweep is made from 2-3 GHz with a total of 2000 samples ($\Delta f = 500KHz$). Also the network analyser has an option to transform the frequency sweep into a time domain representation which for each setup also have been saved.

A.3 Data processing

The frequency sweep corresponding time domain representation is saved as a .csv file including, frequency steps, time steps, magnitude and phase(degree).

The following method is used to calculate the time domain response from the frequency sweep in Matlab.

- Load the .csv data file into matlab.
- Convert the power to amplitude.
- Calculate the baseband I/Q signal from the amplitude and phase.
- Apply hamming window with same length as the baseband signal.
- Calculate the IFFT of the baseband signal and the correct time-axis.
- Calculate the first peak above a given threshold to estimate ToA.
- Mark the correct distance on figures.

A.4 Channel Impulse Responses and Frequency Sweeps

The following results were obtained by using the above procedure. It is seen that for all LOS the error from first peak and the true distance is small, however for test 4 and 5 it can be seen that the first peak is highly attenuated and the peak is detected wrong, the peak-detection threshold is set for -10 dBm (0.1 mW). Both the measured frequency response and time response is shown in pairs, see figs. A.3 to A.8.

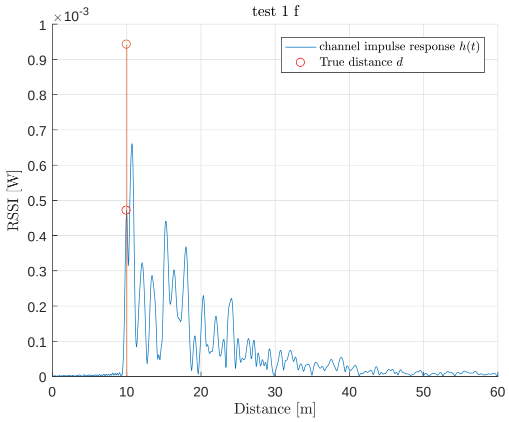

(a) *Channel impulse response, $h(t)$*

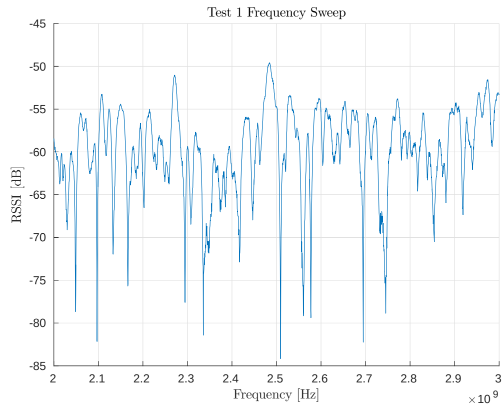

(b) *Frequency sweep for 2-3 GHz $H(f)$*

Figure A.3: *Measured frequency sweep and calculated channel impulse responses test 1, condition is LOS.*

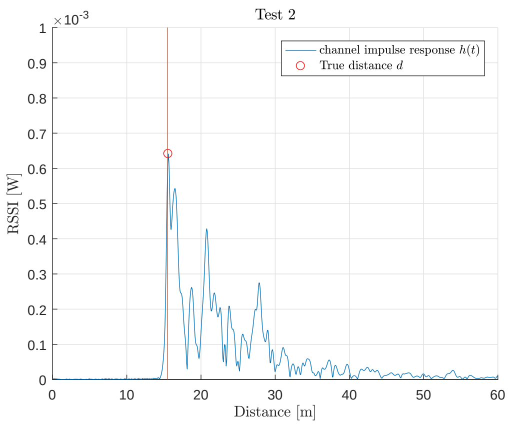

(a) *Channel impulse response, $h(t)$*

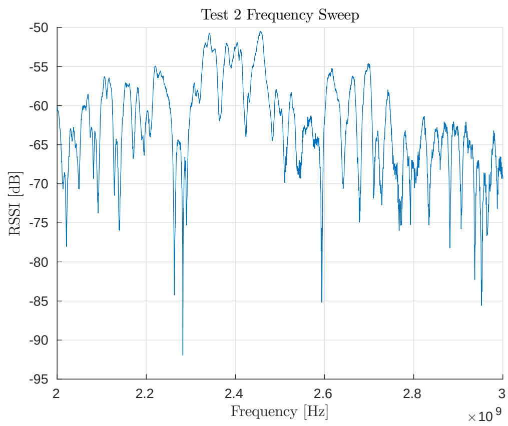

(b) *Frequency sweep for 2-3 GHz $H(f)$*

Figure A.4: *Measured frequency sweep and calculated channel impulse responses test 2, condition is LOS.*

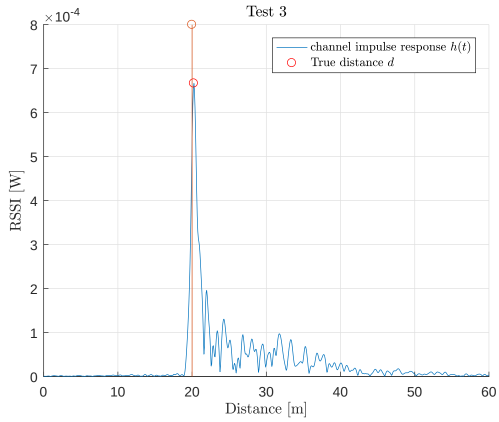

(a) *Channel impulse response, $h(t)$*

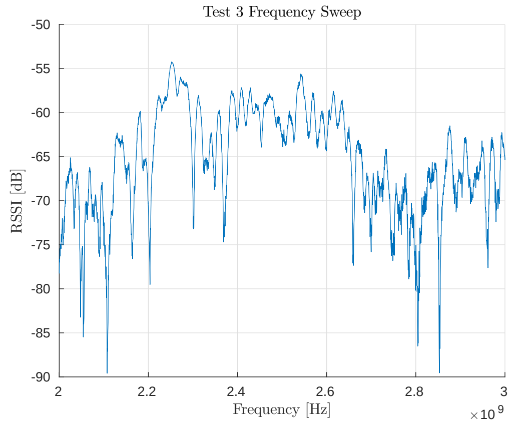

(b) *Frequency sweep for 2-3 GHz $H(f)$*

Figure A.5: *Measured frequency sweep and calculated channel impulse responses test 3, condition is LOS.*

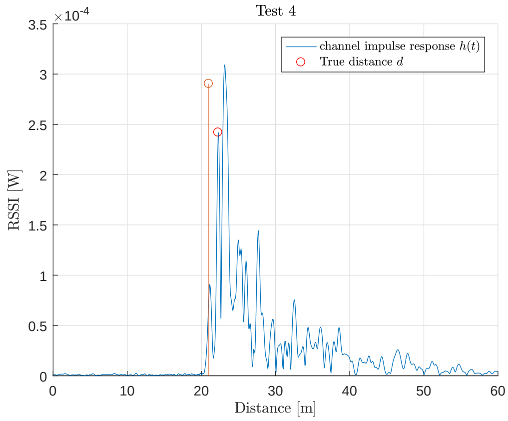

(a) *Channel impulse response, $h(t)$*

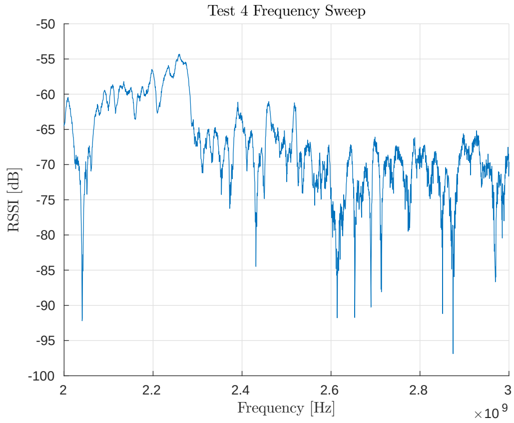

(b) *Frequency sweep for 2-3 GHz $H(f)$*

Figure A.6: *Measured frequency sweep and calculated channel impulse responses test 4, condition is NLOS.*

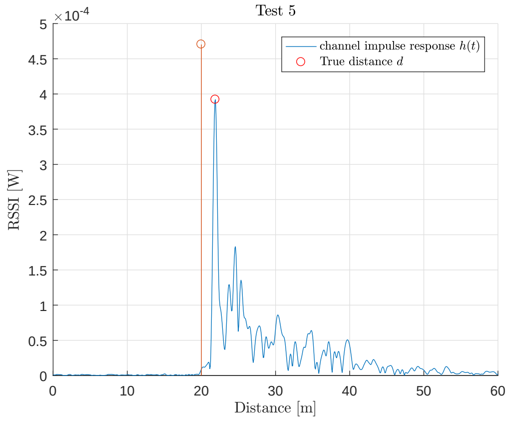

(a) *Channel impulse response, $h(t)$*

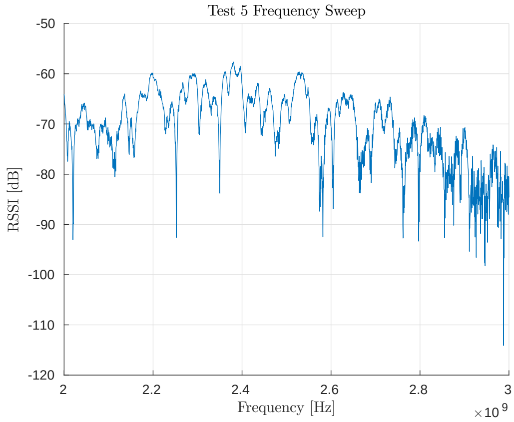

(b) *Frequency sweep for 2-3 GHz $H(f)$*

Figure A.7: *Measured frequency sweep and calculated channel impulse responses test 5, condition is NLOS.*

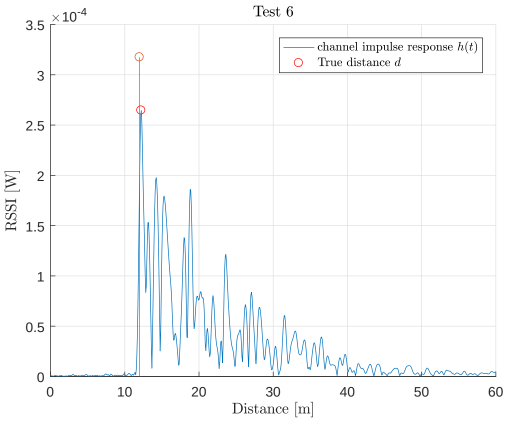

(a) *Channel impulse response, $h(t)$*

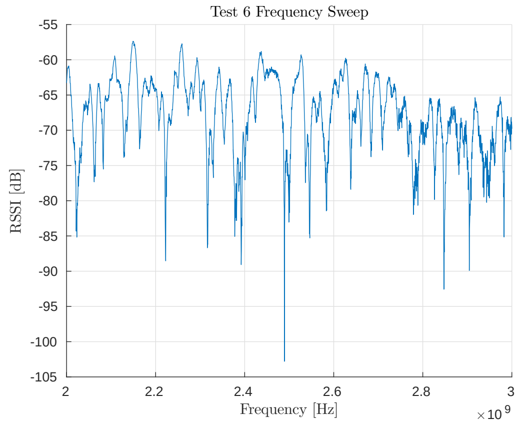

(b) *Frequency sweep for 2-3 GHz $H(f)$*

Figure A.8: *Measured frequency sweep and calculated channel impulse responses test 6, condition is NLOS.*

In the case of NLOS (test 4-6) it is seen that the direct path signal is attenuated in test 4 and 5, however for test 6 the NLOS does not provide noticeable attenuation. In the LOS case, test 2-3 shows that the direct path is the strongest compared with the following delayed reflections. For test 1 however the direct path is not the strongest, but could be explained by the arrival of two reflected paths arriving in the same time delay shortly after first peak.

A.5 Coherence Bandwidth

As the channel is assumed to be WSSUS when measuring, the method used to obtain uncorrelated data could be frequency shifting. This is a result of the channel at a given frequency obtain WSS in the time variable and uncorrelated scattering in the delay variable, however to obtain several uncorrelated scatters frequency hopping is used.

To achieve at least partially uncorrelated data it is important to know how much to changes the frequency, this change is called the coherence bandwidth, where a given correlation value is satisfied. Therefore the frequency correlation function (FCF) is calculated so that the coherence bandwidth can be found.

To calculate the coherence bandwidth different approaches can be used, one is to calculate the Fourier transformation of the power delay profile (PDP). Second method is to calculate the autocorrelation of the measured frequency sweep. To check the coherence bandwidth for an actual bandwidth B in the system a part of the sweep corresponding to the actual bandwidth is used and the autocorrelation for this bandwidth is calculated and averaged for all frequency steps.

Using the second method and calculating the autocorrelation of the frequency bandwidth, the FCF for different bandwidths are found on fig. A.9. The coherence bandwidth has been calculated for all 6 tests using a bandwidth of 40 MHz and 80 MHz.

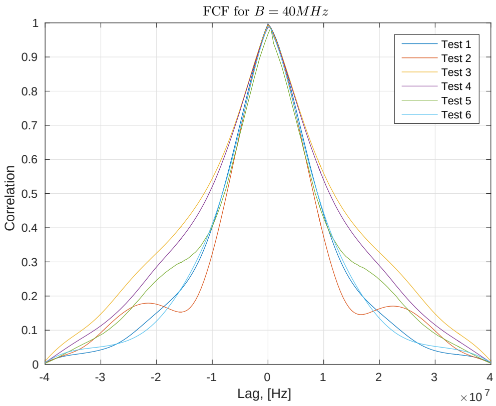

(a) *Bandwidth of 40 MHz.*

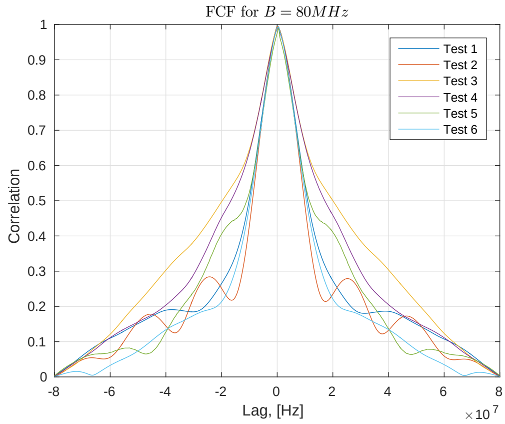

(b) *Bandwidth of 80 MHz.*

Figure A.9: *Frequency correlation function created from test 1-6.*

For a 0.5 correlation level the coherence bandwidth lies between 15-22.5 MHz for the measurements using a 40 MHz bandwidth and using bandwidth of 80 MHz the coherence BW is 18-40 MHz. Therefore if a higher bandwidth is used to obtain data, the difference in frequency, Δf to shift to obtain uncorrelated data is larger.

Appendix B

Impact of Indoor Environment

Sections 2.3.1 to 2.3.3 describes the different input-data which can be obtained from the different characteristics of a wireless channel. These characteristics are easily obtained in an outdoor environment, with few-to-none reflections and obstructions. The same characteristics in an indoor environment is however decreasing the systems ability to locate a tag.

More precisely it is the impact of whether the tag and node is in LOS or NLOS condition, and if reflections are present or not, for more information see section 2.1. The different conditions have a huge impact on the performance and ability to calculate the location of a tag, as multipath will occur in an indoor environment in a smaller or larger scale, see fig. B.1.

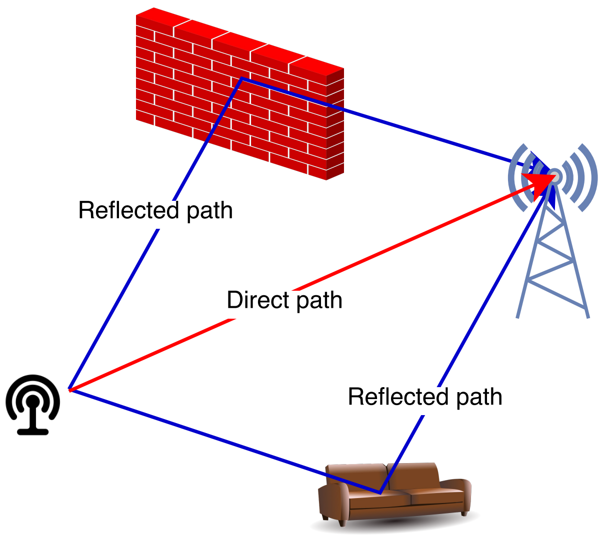

Figure B.1: *Multipath environment, reflections occur on objects. Figure shows LOS condition, as no blocking of direct path.*

The LOS condition in a multipath environment will be described as a reception of the signal with a dominant direct path (DDP), thereby the first arriving signal is the direct path and also the strongest. NLOS can be further divided into two different subcategories, namely non dominant direct path (NDDP) and undetected direct path (UDP). NDDP is generally the same as DDP, the only difference is that the direct path is no longer the strongest, which in some cases might introduce estimation errors. UDP is the case that the direct path is attenuated below receiver sensitivity, thereby not being detected. This could be the case of a wall attenuating the signal, and therefore what looks like the first path arriving, is actually a reflected path.

The received signal is dependent on the channel impulse response (h), meaning a description of the channel the signal is transmitted over. h for the channel found on fig. B.1, is depicted as fig. B.2. An ideal tag is transmitting what is ideally a dirac pulse (δ) and at the node the received signal is represented as the δ transmitted over different paths each with different attenuation (α) and propagation delay (τ), see eq. (B.1). The dirac pulse is an observation happening if the system has infinite B.

$$h(t) = \sum_{i=0}^{K} \alpha_i \cdot \delta(t - \tau_i) \tag{B.1}$$

Where K is the amount of paths.

Equation (B.1) is shown in fig. B.2 as the direct path (red line) and reflected paths (blue lines).

Due to the limitations of the system, the bandwidth can not be infinite and by limiting the bandwidth of a system, the δ pulse instead becomes a pulse shape. This pulse shape assuming a rectangular filter, become a sinc-function, which is dependent on the bandwidth of the transmitted signal. For a bandwidth limited system eq. (B.1) translates into eq. (B.2).

$$h(t) = \sum_{i=0}^{K} \alpha_i \cdot sinc(B \cdot (t - \tau_i)) \tag{B.2}$$

Where B is the bandwidth of the system and K is the amount of paths. Equation (B.2) is shown on fig. B.2 as the black line.

The impact of the pulse shape has a huge impact on especially AoA and ToA methods. AoA as the angle of arrival can change significantly if the direct path and reflected path arrives with small Δt, as discriminating the arrivals becomes difficult. ToA as what is detected as the peak of the first arriving path is different, from the actual direct path (difference between dashed grey and red line, fig. B.2). The following sections will describe and evaluate the problems related to the indoor environment.

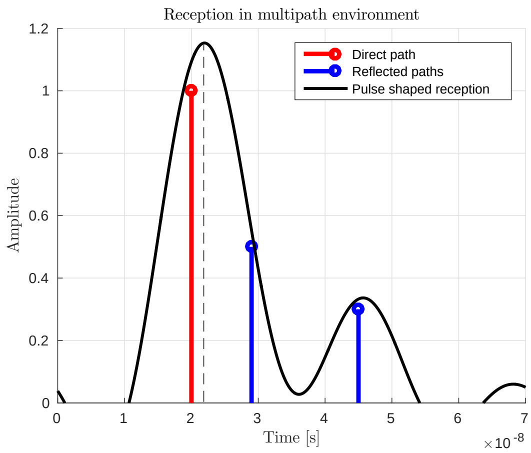

Figure B.2: *Received signal corresponding with fig. B.1. Red line is direct path and blue is different reflected paths.*